Advances in Materials
2019; 8(2): 70-93
http://www.sciencepublishinggroup.com/j/am
doi: 10.11648/j.am.20190802.15
ISSN: 2327-2503 (Print); ISSN: 2327-252X (Online)

Effects of Zn Substitution on Structure Factors, Debye-Waller Factors and Related Structural Properties of the $Mg_{1-x}Zn_xFeNiO_4$ Spinels

Kadhim Ahmed Khalaf[1, *], Ahmed Al-Rawas[2], Abbasher Gismelseed[2], Majid Al-Ruqeishi[2], Salwan Al-Ani[3], Ahmad Al-Jubouri[1], Khamis Al-Ryami[1], Bushra Al-Jaddedi[1]

[1]Department of Mathematical and Physical Sciences, College of Arts and Sciences, University of Nizwa, Nizwa, Oman

[2]Department of Physics, College of Science, Sultan Qaboos University, Al-koud, Oman

[3]Department of Physics, College of Science, University of Baghdad, Baghdad, Iraq

Email address:
kadhimm@unizwa.edu.om (K. A. Khalaf)

[*]Corresponding author

To cite this article:
Kadhim Ahmed Khalaf, Ahmed Al-Rawas, Abbasher Gismelseed, Majid Al-Ruqeishi, Salwan Al-Ani, Ahmad Al-Jubouri, Khamis Al-Ryami, Bushra Al-Jaddedi. Effects of Zn Substitution on Structure Factors, Debye-Waller Factors and Related Structural Properties of the $Mg_{1-x}Zn_xFeNiO_4$ Spinels. *Advances in Materials*. Vol. 8, No. 2, 2019, pp. 70-93. doi: 10.11648/j.am.20190802.15

Received: January 7, 2019; **Accepted**: May 24, 2019; **Published**: June 10, 2019

Abstract: The effects of Zn^{2+} ions substitutions on the Debye-Waller Factors, structure factor and other related structural properties of the $Mg_{1-x}Zn_xNiFeO_4$ (where $0.0 \leq x \leq 1.0$) spinels have been investigated using the XRD, TEM, SEM and FT-IR tools. The $Mg_{1-x}Zn_xNiFeO_4$ samples were prepared using the conventional ceramic solid state sintering techniques at temperatures around 1100°C. The $Mg_{1-x}Zn_xNiFeO_4$ spinels have predominantly inverse type structure with inversion factor, λ in the range 0.69 to 0.36. The X-ray diffraction (XRD) patterns of all compositions showed the formation of cubic spinel structure. The lattice constant "a" increases from 8.3397Å for $MgFeNiO_4$ to 8.3855Å for $ZnFeNiO_4$ spinels. The increases in lattice parameters have been attributed to the replacement of small Mg^{2+} ions (0.66 Å) with the Zn^{2+} (0.74 Å) ions of a larger ionic radius. The IR spectra confirm the existence of two main absorption bands υ_1 and υ_2 in the frequency range of (400–1000 cm^{-1}), arising due to the tetrahedral (A) and octahedral (B) stretching vibrations respectively. Values of both υ_1 and υ_2 decrease as Zn content increases. The scanning electron microscope (SEM) and transmission electron microscope (TEM) images showed aggregates of stacked grains. The normalized XRD intensities of the main (hkl) planes were used in the estimation of the Debye-Waller factor. Values of the Debye-Waller factors were estimated to be in the range (0.77-1.44A^2). The calculated and observed relative intensities and areas of the most related plains to cation distributions (i.e.: the (220), (311), (222), (400), (422), (511) and (440) plains) were obtained by normalizing with respect to the most intensive reflection from the (311) plane. An inverse relation between the ordering, Q and inversion, λ factors exists in these partially inverse spinels. Both Q and λ decrease as Zn content (x) increases in the sample. The cation distributions indicate that the sample, $MgFeNiO_4$ with x=0, λ=2/3 and maximum configurational entropy Sc(=15.876 J/mol, K) should represents the sample of the complete randomness of cation distributions in these spinels and can be written as $(Mg_{1/3}Fe_{2/3})[Mg_{2/3}Fe_{1/3}Ni_{3/3})O_4$. In general the variation of the different structural parameters with Zn content lie on two different regions, the first region for x values (0.0-0.6) the "highly normal" and the second region for x values (0.6-1.0) the "highly inverse" type structure.

Keywords: XRD, TEM, SEM, FTIR, Structure Factor, Debye Waller Factor, Order Parameter

1. Introduction

Spinel ferrites are characterized by many unique magnetic and electrical properties. The high electrical resistivity gives rise to low eddy current and dielectric losses. Ferrites have also been used in other important applications such as information storage systems, gas sensors, microwave devices and magnetic recording and electronic industries [1-2]. The properties of the spinel systems depend on many factors such

as the preparation techniques, heat treatment processes, chemical compositions and the cations distributions among the tetrahedral (A-) and octahedral (B-) sublattices sites. The wide variations in these properties are direct reflection of their ability to accommodate and distribute a variety of cations among their two subsites the (A-) and (B-) sites. The distributions of cations among the A- and B- sites depend on their affinity for both positions, which depends upon many factors such as the stabilization energy, ionic radii, size of the interstices, electronegativity, coulomb energy, the types of synthesis techniques and conditions during the synthesis process [2]. The anions (such as O, S, …) in the spinel structure form 96 interstices. These interstices are distributed over the tetrahedral and octahedral sites as; 64 at the A- sites and 32 at the B- sites. Not all the 96 interstices are occupied by cations, only 8 of the tetrahedral and 16 of the octahedral interstices are known to be occupied by cations. The general formula for the cation distributions in spinels can be written as $(X_{1-\lambda}Y_{\lambda})_A[X_{\lambda}Y_{2-\lambda}]_BO_4$ where X^{2+} and Y^{3+} represent transition metal ions. The factor λ represents the fraction of Y^{3+} metals at the A-sites, which equals to 0 for normal spinel and 1 for the inverse spinels. For mixed spinels the inversion factor λ values lies between 0 and 1. The $ZnFe_2O_4$ [3], $CdFe_2O_4$ [4] ferrites and $ZnCr_2O_4$ chromites [5] have the normal spinel type structure, in which the Zn^{2+} and Cd^{2+} ions occupy the A-sites while the Fe^{3+} and Cr^{3+} ions occupy the B-sites. The Nickel ferrites, $NiFe_2O_4$ have the inverse spinel structure [3], in which the Fe^{3+} ions occupy the tetrahedral sites where the octahedral B-sites are occupied by the Ni^{2+} and Fe^{3+} ions. The Magnesium ferrite, $MgFe_2O_4$, has the mixed spinel structure [6-7], in which the degree of inversion depends on many factors such as the preparation technique and the heat treatment in particular. In principle, the large (small) cations should occupy the largest (smallest) sites, the octahedral (tetrahedral) sites. Since the trivalent cations are generally smaller than the divalent ones, therefore, there should be some tendency for the trivalent cations to reside on the smallest sites, the tetrahedral sites, leading to the inverse or partially inverse type structure. This factor works in opposite direction of the electric charge factor; that the high (low) electrical charge causes the cations to occupy the larger (smaller) coordination number, the octahedral (tetrahedral) sites [8] leading to the normal (inverse) type structure.

The effects of replacing Fe^{3+} ions with trivalent ions such as Cr^{3+}, Ni^{3+} and Al^{3+} ions have been extensively studied by many workers. It has been well established that Cr^{+3}, Ni^{3+} and Al^{3+} ions have strong tendency to reside at the octahedral sites while the Zn^{2+} and Cd^{+2} ions have strong preference to reside on the tetrahedral sites. Other cations such as the Fe^{3+}, Co^{2+}, Mn^{2+} and Mg^{2+} cations can be present at both sites [9-10]. The cation distributions among the A- and B- sites depends on many factors such as; the composition, temperature, pressure, ionic charge, ionic radius, the crystal field and the anion polarization and the electronegativity [11]. The Mossbauer measurements reveal that the cation distributions in the present $Mg_{1-x}Zn_xFeNiO_4$ samples have the mixed spinel type structure with an inversion factor, λ, in which the Mg^{+2}, Zn^{+2} and Fe^{+3} cations reside at the A- and B-sites while the Ni^{+3} ions reside at the B- sites [12].

The Debye-Waller factor (DWF) provides an acceptable treatment to reduce the negative effects of the attenuation of X-ray diffracted intensities, which is usually caused by thermal vibrations of the atoms about their mean positions [13]. The temperature variation of the DWF for alkali and nobel metals have been reported [14]. The DWF have been calculated for five FCC metals: copper, silver, gold, aluminum and nickel [15, 16] and for three bcc metals: sodium, α-iron and chromium [17-19]. The Debye-Waller factor of molybdenum has been determined by the powder neutron diffraction technique with a double-axis neutron diffractometer [20]. The DWF is related to most of the material properties such as the melting point, electrical conductivity, heat capacity, elastic constants, sound velocities, lattice instabilities, neutron scattering, the mean-square displacement and the effective Debye temperature. Values of the DWF have been calculated using the integrated intensities of the Bragg reflections in the diffracted X-ray spectrum.

The aims of this study are to account for the influence of the Zn^{2+} ions substitutions on the structural properties of the $Mg_{1-x}Zn_xFeNiO_4$ spinels for ($0 \leq x \leq 1.0$) using nondestructive tools such as the X-ray diffraction (XRD), infrared spectroscopy (IR), transmission (TEM) and scanning electron microscopy (SEM) tools. Moreover, theoretical calculations of the Structure factors, Debye-Waller factors and their related structural parameters have also been conducted.

2. Experimental

The $Mg_{1-x}Zn_xFeNiO_4$ spinel ferrites (where x= 0.0, 0.2, 0.4, 0.6, 0.8 and 1.0) were prepared by the conventional double sintering ceramic technique as described earlier [21]. High purity powders of MgO, ZnO, Ni_2O_3 and Fe_2O_3 oxides were weighed carefully to have the desired stoichiometric proportions and mixed in agate mortar. The appropriate mixtures were first sintered at 1000°C for 24 h in air medium followed by slow cooling to room temperature. The powder then remixed and ground once more to promote homogeneity. The powders were sintered at 1150°C for 24 h followed by natural cooling to room temperature. The probable form of the chemical reactions are expected to be of the following form:

$$(1-x)MgO + x\,ZnO + 0.5\,(Fe_2O_3) + 0.5\,(Ni_2O_3) \rightarrow Mg_{1-x}Zn_xFeNiO_4 \quad (1)$$

The single-phase spinel structure was confirmed by the x-ray diffraction spectrum of these samples. The X-ray diffractograms were recorded at room temperature using Philips X-ray diffractometer (model PW1820) with CuKα radiation (λ=1.5404Å). The scan's range was kept the same for all samples ($2\theta=10^o$-100^o) using a step size of (0.02^o) with a sampling time of (2s). The XRD scans were done for only six samples (x= 0.0, 0.2, 0.4, 0.6, 0.8 and 1.0). Samples for IR

spectra scanning were prepared by mixing small quantity of the powder of the samples with solid KBr. The mixed powder was then pressed at 10 tons/cm^2 by a hydraulic press to produce thin cylindrical samples of 1.3 cm in diameter. The IR measurements were recorded at room temperature in the range from 400 to 4000 cm^{-1} using PERKIN-ELMER-1430 infrared spectrophotometer. The microstructure and sample surface morphology were examined with analytical scanning electron microscope (ASEM) model JSM-6510LA-JEOL and transmission electron microscope model JEM-1400-JEOL. Details of the experimental techniques can be found in reference [22].

3. Results and Discussions

3.1. The X-Ray Diffraction Analysis

The X-ray diffraction spectra of the $Mg_{1-x}Zn_xFeNiO_4$ spinels are shown in Figure 1. All samples showed clear XRD reflections from the plains (220), (311), (222), (400), (440), (422), (511), (620) and (533). This can be taken as a good indication of the formation of the single phase cubic spinel structure with the Fd3m space group. These reflections agree quite well with powder reflections of the majority of the spinel systems [23]. The Mossbauer tool has been used to estimate the cation distributions and other related structural and magnetic parameters [12]. These analysis indicate that these spinels are a mixture normal-inverse spinels and the degree of inversion for the pure $MgFeNiO_4$ and $ZnFeNiO_4$ spinels was determined to be round 0.69 and 0.36 respectively. The lattice parameter, "a_{hkl}" at each angle of reflection, θ_{hkl} for the various (hkl) plains have been calculated using Bragg's diffraction law;

$$\left.\begin{aligned} n\,\lambda = 2\,d_{hkl}\,sin\,\theta_{hkl} \\ a_{hkl} = \frac{\lambda\sqrt{h^2+k^2+l^2}}{2\,sin\,\theta_{hkl}} \end{aligned}\right\} \quad (2)$$

Values of the d_{hkl} plane spacing and the lattice parameter, a_{hkl} are calculated and presented in Table 1 as a function of the Miller indices (hkl) and sin(θ_{hkl}). The Nelson-Riley function (N-R-F) method was used for accurate determination of the true values of the lattice parameters, a_{exp}. In this method the estimated values of a_{hkl} for each sample will be plotted versus Nelson-Riley function, F(θ) [23]; which is given as;

$$F(\theta) = \frac{1}{2}\left(\frac{\cos^2\theta}{\sin\theta} + \frac{\cos^2\theta}{\theta}\right) \quad (3)$$

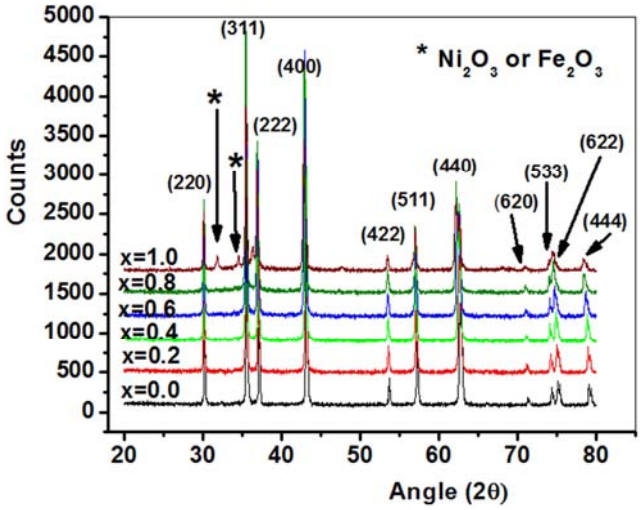

Figure 1. *The X-ray diffraction spectra for the $Mg_{1-x}Zn_xFeNiO_4$ spinels.*

These plots form straight lines with negative slopes, The accurate lattice constants "a_{exp}" values were obtained by the least square fitting of the a_{hkl} values versus F(θ) followed by extrapolation to F(θ)=0 at θ=90^o as shown in Figure 2. The extrapolated values of the lattice constant, a_{exp} were presented in Table 2 as a function of the Zn content in the sample. The true values of the lattice constant, a_{exp} were found to be 8.3594Å and 8.4096Å for the $MgFeNiO_4$ and $ZnFeNiO_4$ samples respectively. The increases in the a_{exp} values can be justified on the basis of the ionic radii differences, where smaller Mg^{+2} (0.66Å) cations have been replaced by larger Zn^{2+} (0.74Å) cations. These values agree with those reported [12] for the similar samples $Mg_{1-x}Zn_xFeNiO_4$ spinels using Rietveld method to be 8.3397Å for $MgFeNiO_4$ and 8.3855Å for $ZnFeNiO_4$. These values agree with those reported [12] for the similar samples $Mg_{1-x}Zn_xFeNiO_4$ spinels using Rietveld method to be 8.3397Å for $MgFeNiO_4$ and 8.3855Å for $ZnFeNiO_4$.

Table 1. *The inter spacing of the different (hkl) planes of the $Mg_{1-x}Zn_xFeNiO_4$ spinels.*

x	(hkl)	Sin(θ)	d- spacing (A)	a_{hkl} (A)
	220	0.261104	2.949787	8.343258
	311	0.306135	2.515881	8.344234
	222	0.318929	2.414961	8.365671
0.0	400	0.368283	2.091326	8.365304
	422	0.451973	1.704083	8.348268
	511	0.479424	1.606511	8.347675
	440	0.521183	1.477791	8.359647
	220	0.260457	2.957111	8.363974
	311	0.305444	2.521574	8.363115
	222	0.318318	2.419596	8.381726
0.2	400	0.36765	2.094926	8.379704
	422	0.451168	1.707126	8.363176
	511	0.47854	1.609478	8.363094
	440	0.520358	1.480135	8.372906

x	(hkl)	Sin(θ)	d- spacing (A)	a_{hkl} (A)
	220	0.260424	2.957485	8.365029
	311	0.305328	2.522535	8.366303
	222	0.318062	2.421543	8.388472
0.4	400	0.367275	2.097065	8.38826
	422	0.450783	1.708582	8.37031
	511	0.478172	1.610717	8.369533
	440	0.519679	1.482068	8.383844
	220	0.260339	2.958453	8.367768
	311	0.30523	2.523342	8.368978
	222	0.31751	2.425752	8.403052
0.6	400	0.366625	2.100782	8.403127
	422	0.450573	1.70938	8.374216
	511	0.47789	1.611669	8.374476
	440	0.518852	1.484432	8.397218
	220	0.260152	2.960583	8.373792
	311	0.305003	2.525224	8.375222
	222	0.31683	2.430957	8.421082
0.8	400	0.365846	2.105259	8.421036
	422	0.450257	1.710578	8.380087
	511	0.477559	1.612784	8.380271
	440	0.517905	1.487145	8.412561
	220	0.259986	2.962471	8.379133
	311	0.304833	2.526627	8.379873
	222	0.316624	2.432541	8.426568
1.0	400	0.365607	2.106631	8.426523
	422	0.450126	1.711078	8.382534
	511	0.477306	1.613641	8.384727
	440	0.517567	1.488118	8.418066

The present results agree with those reported for other spinel systems such as $ZnFeCrO_4$ as (a=8.3764Å) [21], $MgFeCrO_4$ as (a=8.369Å) [24, 26], $CoFeCrO_4$ as (a=8.362Å) [25], $Co_{0.5}Zn_{0.5}Fe_2O_4$ as (a=8.407Å) [27] and $Co_{0.5}Zn_{0.5}Al_{0.2}Fe_{1.8}O_4$ as (a=8.37Å) [28].

Values of the ionic radii at the tetrahedral and octahedral sites can be calculated using the following relations [29];

$$\left.\begin{aligned} r_A &= \left(r_{Mg^{2+}}\right)C^A_{Mg^{2+}} + \left(r_{Zn^{2+}}\right)C^A_{Zn^{2+}} + \left(r_{Fe^{3+}}\right)C^A_{Fe^{3+}} \\ r_B &= \frac{\left(r_{Mg^{2+}}\right)C^A_{Mg^{2+}} + \left(r_{Zn^{2+}}\right)C^A_{Zn^{2+}} + \left(r_{Fe^{3+}}\right)C^A_{Fe^{3+}} + \left(r_{Ni^{3+}}\right)C^A_{Ni^{3+}}}{2} \end{aligned}\right\} \quad (4)$$

Where C_n and r_n represent the concentration and radius of the cations at the A- and B- sites respectively. Values of C_n for the concerned cations have been taken from the cation distributions determined from Mossbauer study [12]. Values of the cation radius for Mg^{2+}, Zn^{2+}, Fe^{3+} and Ni^{3+} ions have been taken as 0.66, 0.74, 0.67 and 0.70Å respectively [30].

The calculated values of the average cation radius r_A and r_B sites are shown in Table 2. It is clear from Figure 3 that values of r_A and r_B vary nonlinearly with Zn content. The variations of r_A and r_B reflect the changes of the cation distribution at the tetrahedral and octahedral sites, which can be explained as the Zn^{2+} (Mg^{+2}) concentration at the A- and B- sites increases (decreases) a redistribution of the cations and migration of some of the Fe^{3+} ions from the A- to the B-sites. This results in a reduction of the inversion factor, λ of the concerned samples. The overall resultant changes in the cation distribution were reflected in the increase of the lattice parameter a_{exp} values with Zn content. Similar results have been shown by other related spinels such as $Mg_{1-x}Zn_xFeCrO_4$ [31], $Cu_{1-x}Zn_xFeCrO_4$ [32], $Cu_{1-x}Zn_xFe_2O_4$ [33] and $CrCo_xNi_{1-x}FeO_4$ [34] and $Ni_{1-x}Zn_xFeCrO_4$ [35].

Table 2. *The inter-ionic radii, the lattice constants, oxygen position parameter, the inter-ionic bond lengths of the $Mg_{1-x}Zn_xFeNiO_4$ spinels.*

x	aexp(A)	ath(A)	rA (A)	rB (A)	ravg (A)	uA	uB	uavg	Reff (A)	RA (A)	RB (A)	Ravg (A)
0.0	8.3594	8.3681	0.6669	0.6816	0.6742	0.3914	0.3784	0.3849	1.9909	1.9531	2.0104	1.9818
0.2	8.3690	8.3793	0.6821	0.6820	0.6820	0.3923	0.3786	0.3855	1.9931	1.9641	2.0082	1.9862
0.4	8.3804	8.3913	0.6973	0.6824	0.6898	0.3931	0.3789	0.386	1.9953	1.9740	2.0071	1.9905
0.6	8.3949	8.4104	0.7099	0.6841	0.6970	0.3937	0.3791	0.3864	1.9977	1.9855	2.0076	1.9965
0.8	8.4080	8.4198	0.7127	0.6907	0.7017	0.3937	0.3787	0.3862	1.9989	1.9835	2.0122	1.9979
1.0	8.4096	8.4201	0.7148	0.6976	0.7062	0.3938	0.3779	0.3859	1.9986	1.9794	2.0148	1.9971

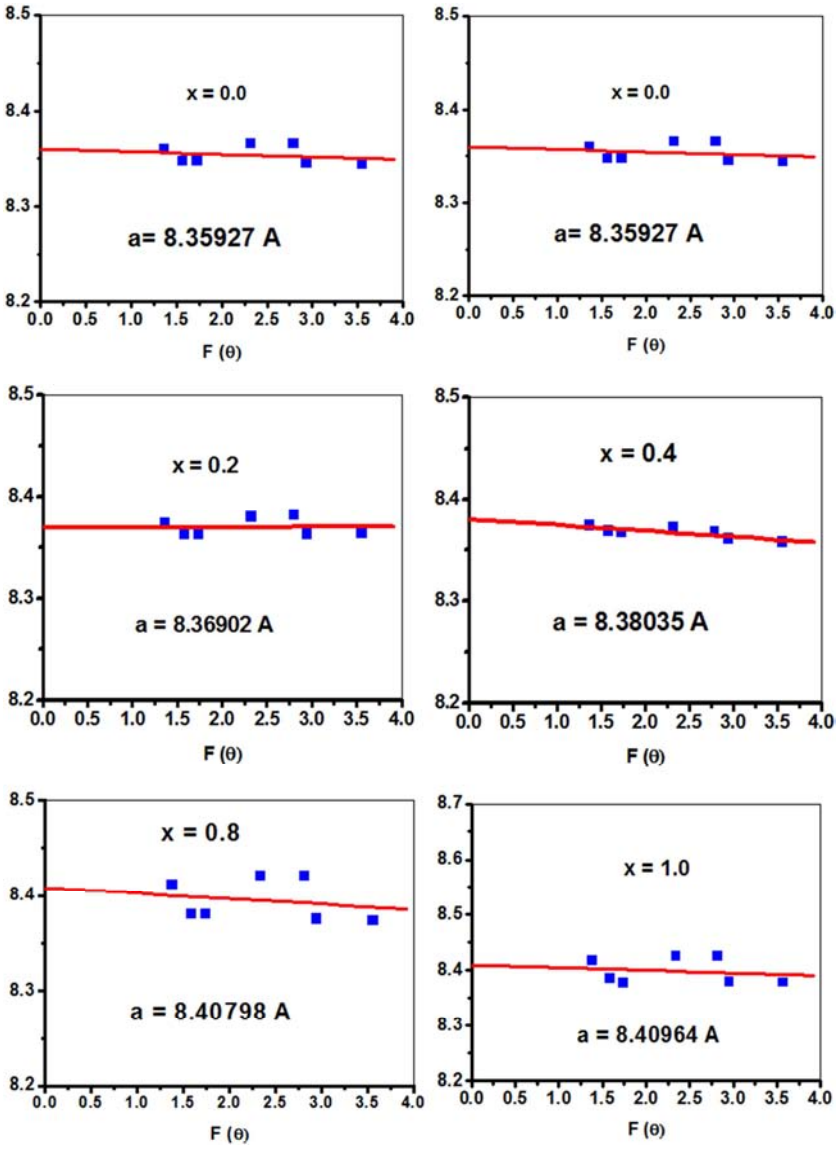

Figure 2. *Values of lattice constants, a_{hkl} versus F(θ) for the $Mg_{1-x}Zn_xFeNiO_4$ spinels.*

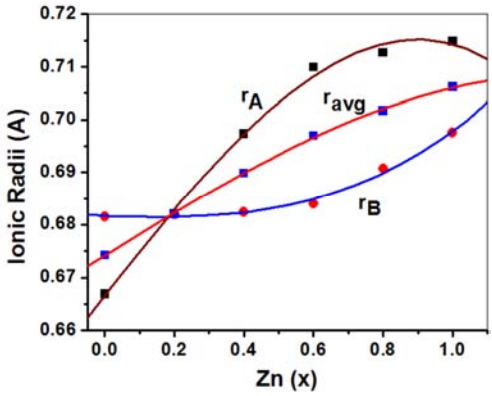

Figure 3. *The ionic radii r_A and r_B at the A- and B- sites versus Zn content (x) for the $Mg_{1-x}Zn_xFeNiO_4$ spinels.*

Most of the structural parameters such as the cations-anions bonds R_A and R_B at the A- and B- sites respectively and the theoretical values of the lattice constant, a_{th} and many others parameters depende on the value of the oxygen positional parameter u. Accordingly, it has to be estimated first. The u parameter is directly related to the average ionic radii at the tetrahedal and octahedral sites through the following relations [36];

$$\left.\begin{aligned} u_A &= \frac{r_A+R_o}{\sqrt{3}a_{exp}} + \frac{1}{4} \\ u_B &= \frac{5}{8} - \frac{r_B+R_o}{a_{exp}} \\ u_{avg} &= \frac{(u_A+u_B)}{2} \end{aligned}\right\} \quad (5)$$

where r_A and r_B represent the average cationic radius at the tetrahedarl and octahedral respectively. The anion radius R_o has been taken to be 1.38Å [30]. Figure 4 shows the relation between u_{avg} and λ with x for the $Mg_{1-x}Zn_xFeNiO_4$ spinels. It is clear that values of u_{avg} increase as x increases, it reaches its maximum at about x=0.6 then it tends to saturate. The inset in Figure 4 shows the relation between u_{avg} and λ. u_{avg} increses first reaching its maximum at about λ=0.43 then it

decreases fast as λ increases. It is clear that values of u_{avg} fall in two straight line segments with different slopes. The first segment is in the range (0.0 – 0.6) and the second is in the range (0.0 – 1.0). The two regions cross at about x=0.6. The present results differ from those reported for perfect normal and perfect inverse spinels such as the Zn- and Ni- spinels [3]. These behaviors are supported by the variation of the inversion factor λ with x, which also lies in two different regions crossing at about the same point. These characteristics are related to the relative structural phase changes in the mixture spinel type structure. Values of u_{avg} are shown in Table 2 as a function of Zn content (x). Values of u_{avg} for the $Mg_{1-x}Zn_xFeNiO_4$ spinels lie in the range (0.3780–0.3801) compare quite well with those reported for a large number of spinels (0.375–0.395) [37]. The u_{avg} values for the present spinels (like most of the known spinels) are higher than the ideal value (u=0.375), which is necessary to obtain the ideal cubic closest-packing for the anions in the spinel unit cell. The deviation from the ideal value comes as a consequence of the adjustment of the unit cell dimensions to accommodate the differences in the relative effective radii of cations at the tetrahedral and octahedral sites. These will cause the oxygen anions to be displaced away (toward) the nearest tetrahedral (octahedral) cation in the [111] direction increasing (decreasing) the tetrahedron (octahedron) sizes at the expense of each other [38]. The sudden change happened when part of the Zn^{2+} cations move from A- sites to B-sites in the samples with x=0.8 and x=1.0 in particular. Values of u_{avg} for the $Mg_{1-x}Zn_xFeNiO_4$ spinels compare well with those reported for the related $MgFe_{1-x}Cr_xO_4$ spinels [21].

The bond lengths R_A, R_B, R_{avg} and the effective bond lengths, R_{eff} can be evaluated using the following relations [23, 36];

$$\left.\begin{aligned} R_A &= a_{exp}\left(u_{avg} - \frac{1}{4}\right)\sqrt{3} \\ R_B &= a_{exp}\sqrt{3\,{u_{avg}}^2 - \frac{11}{4}u_{avg} + \frac{43}{64}} \\ R_{avg} &= \left(\frac{R_A + R_B}{2}\right) \\ R_{eff} &= \frac{R_A + R_B}{\sqrt{R_A + R_B}} \end{aligned}\right\} \quad (6)$$

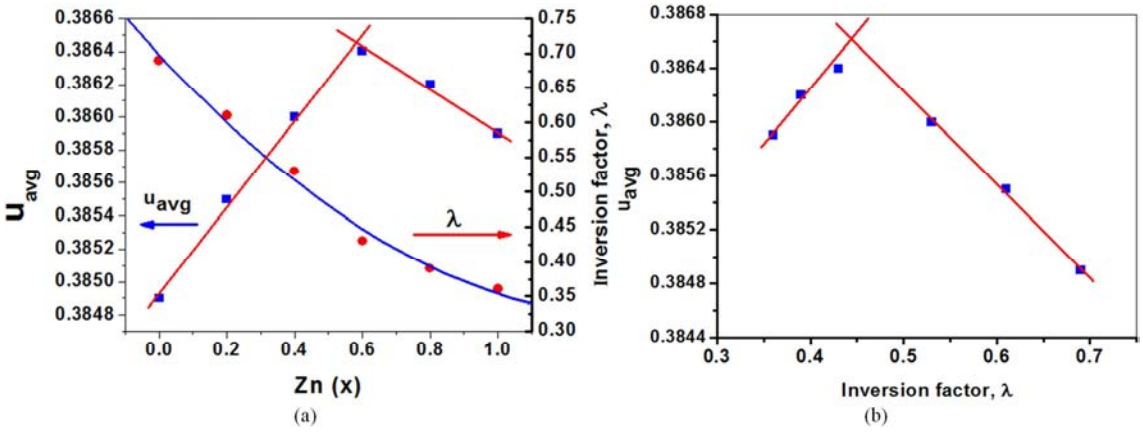

Figure 4. *(a): The oxygen position parameter, u_{avg} and inversion factor, λ versus Zn content (x) for the $Mg_{1-x}Zn_xFeNiO_4$ spinels. (b): shows u_{avg} versus the inversion factor, λ.*

The calculated values of R_A, R_B, R_{avg} and R_{eff} bonds are shown in Table 2. The values of R_A (R_B) increase (decrease) in the range x=0 to x=0.6, then they decrease (increase) for x > 0.6. The average values of R_A and R_B increase smoothly as x increases as shown in Figure 5. The bond lengths at octahedral sites, R_B are higher than that of the tetrahedral sites, R_A. This has been interpreted as more covalent bondings of cation-anion at the A-sites than that at the B-sites [38]. These results support the interpretation that correlates the decrease in the bond length to the increased covalent bonding. The nature of variations of R_A and R_B with x confirm the existence of two distinct features in these spinels. These behaviors have been reflected in the force constant strengths, which have been caused by the bond stretching frequencies at the A- and B- sites. Similar results have been shown by other spinel system such as $Zn_xCu_{1-x}FeCrO_4$ spinels [32]. The theoretical values of the lattice parameter, a_{th} can be evaluated using the following relations [37];

$$a_{th} = \frac{8}{9}\left(\sqrt{3}R_A + 3R_B\right) \quad (7)$$

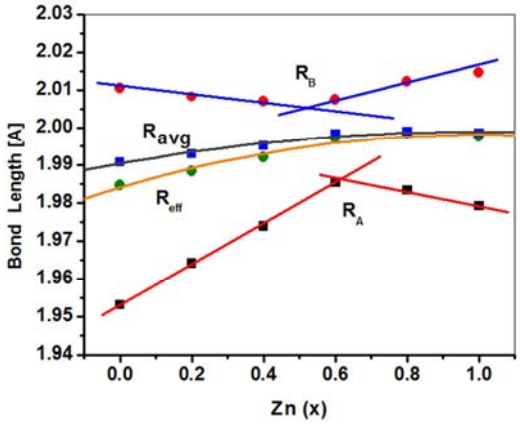

Figure 5. *The bond lengths R_A, R_B, R_{avg} and R_{eff} vs. Zn (x) for $Mg_{1-x}Zn_xFeNiO_4$ spinels.*

Values of the experimental and theoretical lattice constants are shown as a function of the Zn contents in Figure 6. In spite of the fact that the theoretical lattice parameters are higher than those of the experimental, a very good agreement between the experimental and theoretical values of the lattice constant "a". Figure 6 shows also the inversion factore λ as a function of the Zn content.

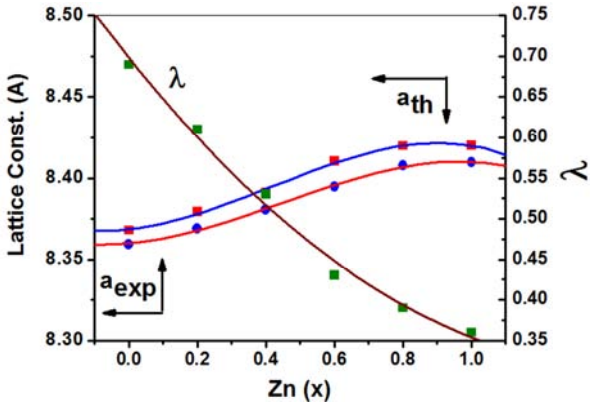

Figure 6. *The lattice constants, a_{exp} and a_{th} versus Zn content (x) for the $Mg_{1-x}Zn_xFeNiO_4$ spinels.*

The tolerance factor (T. F.) provides an indication of the distortion of the crystalline structure. The (T. F) for cubic structure can be calculated using the following relation [39];

$$\text{T. F.} = \frac{1}{\sqrt{3}}\frac{(r_A+r_O)}{(r_B+r_O)} + \frac{1}{\sqrt{2}}\frac{r_O}{r_B+r_O} \quad (8)$$

This approaches unity if the ideal spinel cubic structure was met. Values of the calculated T. F. are shown in Table 3. It is clear that they are not equal to unity indicating the presence of some sort of distortion of the structure in these spinels. Moreover, values of T. F. lie into two straight lines with different slopes as shown in Figure 7. The distortion increases as the Zn content increases reaching maximum for x=0.6, It seems that the distortion increases as the Zn concentration on the A-sites increases. This might be caused by the large radius of the Zn^{2+} cations. The distortion starts decreasing sharply when the Zn^{2+} cations start residing on the octahedral sites.

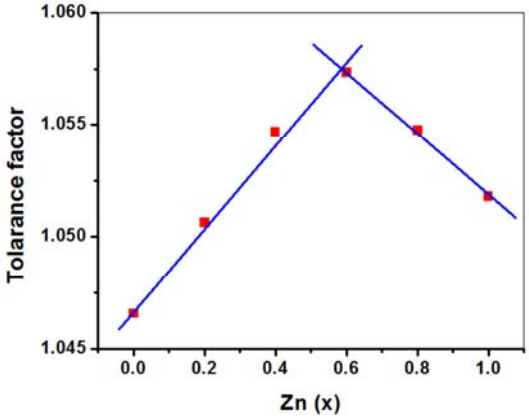

Figure 7. *Values of tolerance factor versus Zn content (x) for the $Mg_{1-x}Zn_xFeNiO_4$ spinels.*

The densities and porosity in these samples can be calculated using the following equations;

$$\left.\begin{aligned} d_{exp} &= \frac{m}{V} \\ d_{XRD} &= \frac{ZM}{VN_A} \\ p &= \left(\frac{d_{XRD}-d_{exp}}{d_{XRD}}\right)100\% \end{aligned}\right\} \quad (9)$$

where d_{exp} and d_{XRD} represent the experimental and theoretical densities respectively, while p represent the porosity. The m and V represent the mass and volume of the cylindrical pellets respectively. The Z, M and N_A represent the number of molecules per unit cell (=8), average molecular mass and the Avogadro's number respectively. Values of the density and porosity have been calculated and shown in Table 3 as a function of Zn content in the sample. The density increases with increasing Zn content as shown in Figure 8-a. This might be caused by the molecular mass differences between Zn (65.926 g/mole) and Mg (23.985 g/mole).

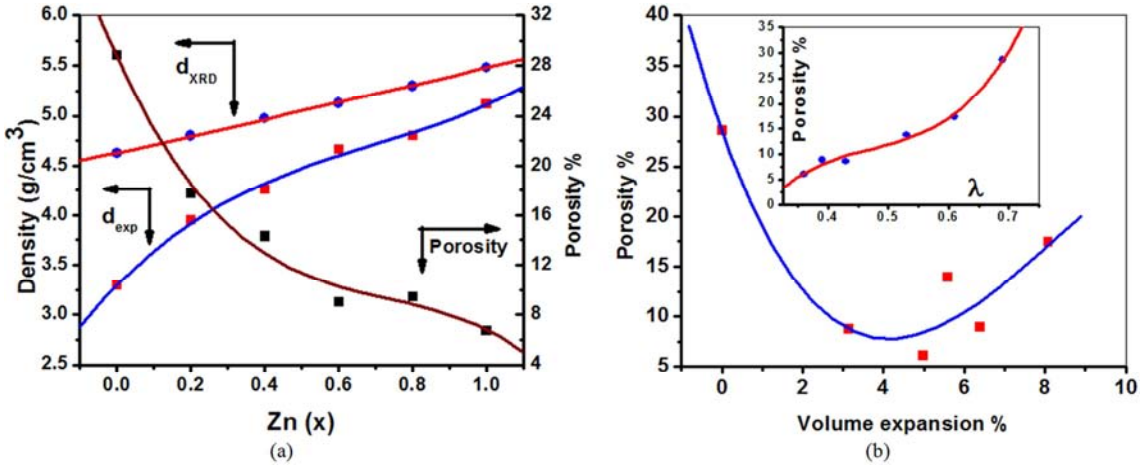

Figure 8. *(a): Values of densities d_{XRD}, d_{exp} and the Porosity versus Zn content in $Mg_{1-x}Zn_xFeNiO_4$ spinels. (b): The porosity versus sample volume expansion. The inset shows the porosity versus inversion factor.*

Table 3. *The densities, porosity, pellets diameter and tolerance factor of the $Mg_{1-x}Zn_xFeNiO_4$ spinels.*

x	Densities		Porosity (%)	Pellet's parameters			Tolerance
	d_{exp} (g/cm^3)	d_{XRD} (g/cm^3)		Width (cm)	Radius (cm)	Volume (cm^3)	Factor
0.0	3.2931	4.6129	28.6108	0.078	0.6345	0.0987	1.0466
0.2	3.9485	4.7832	17.4508	0.155	0.6070	0.1795	1.0506
0.4	4.2601	4.9491	13.9223	0.136	0.6015	0.1546	1.0547
0.6	4.6640	5.1080	8.6921	0.119	0.5900	0.1302	1.0573
0.8	4.7980	5.2678	8.9175	0.145	0.5975	0.1627	1.0548
1.0	5.1166	5.4482	6.0871	0.136	0.5895	0.1485	1.0518

The theoretical (true) densities, d_{XRD}, are higher than the experimental (bulk) densities, d_{exp}, for all samples. The d_{exp} values form (71 to 94%) of d_{XRD}. The differences between values of the densities can be attributed to the pores creation in the samples during the sintering processes at high temperatures. The apparent porosity in these samples decrease with increasing the inversion factors shown in Figure 8-b. This behaviours might convey that the more inverse the spinel the more pores and voids and less density the sample. Similar results have been reported for other spinels such as the $Mg_{1-x}Zn_xFe_2O_4$ [21], $Mg_{1-x}Zn_xFeCrO_4$ [22], $Co_{1-x}Ni_xFe_2O_4$ [26], $Cu_{1-x}Zn_xFe_2O_4$ [33], $NiFe_{2-x}Cr_xO_4$ [40], $NiFe_{2-x}Al_xO_4$ [41] and $Co_{1-x}Mg_xFe_2O_4$ [42], $Ni_xCo_{1-x}Fe_2O_4$ [43] and $Zn_{1-x}Co_xFe_2O_4$ [44] spinels. The differences in the behaviuors between the two similar spinels the $Mg_{1-x}Zn_xFeNiO_4$ and $Mg_{1-x}Zn_xFeCrO_4$ lie in the porosity behaviours, which decreases in the first and increases in the second due to the opposite effects of the Ni^{3+} and Cr^{3+} cations in the sample.

3.2. The Crystallite Sizes

The average values of the crystallite sizes in the $Mg_{1-x}Zn_xFeNiO_4$ spinels have been estimated using the Debye Scherrer's, (D-S) [23], Williamson-Hall, (W-H) [45] and the size-strain, (S-S) [23, 46] methods. The S-S method is characterized by giving less weight to data obtained from the high angle reflections [47].

$$\left.\begin{aligned} \beta &= \frac{K\lambda}{\cos\theta D_{D-S}} \\ \beta cos\theta &= \epsilon\, 4sin\theta + \frac{K\lambda}{D_{W-H}} \\ \left(\frac{d_{hkl}\beta_{hkl}cos\theta_{hkl}}{\lambda}\right)^2 &= \frac{K}{D_{S-S}}\left(\frac{d_{hkl}^2\beta_{hkl}cos\theta_{hkl}}{\lambda}\right) + \left(\frac{\epsilon}{2}\right)^2 \\ \epsilon_{rms} &= \frac{\epsilon}{2\sqrt{2\,\pi}} \end{aligned}\right\} \quad (10)$$

where K is constant has been taken as 0.89, β represent the peak width at half maximum (FWHM) and ε is the apparent strain, which can be related to the root-mean-square strain, ε_{rms}. Values of the crystallite sizes D_{D-S}, D_{W-H} and D_{S-S} were estimated by plotting the (L. H. S.) versus the first term in the (R. H. S.) of equation (9). The crystallite sizes and the microstrain in these spinels were deduced from the slope and the intercept respectively. The instrumental effect errors on the diffraction peak broadening were ignored in these calculations. The estimated average values of D_{D-S}, D_{W-H} and D_{S-S} were estimated to be 31, 87 and 59 nm respectively. Table 4 shows values of the crystallite sizes versus the Zn content. It is clear from Figure 9 that values of the crystallite sizes increase first passing through broad maximum as Zn content increases then they decrease. Similar results have been reported for the $NiFe_{2-x}Cr_xO_4$ [40] and $MgFe_{2-x}Cr_xO_4$ [24] spinels. It is clear that values of D_{W-H} are higher than those of D_{D-S} and D_{S-S}. Quite similar behaviours have been reported for the $Co_{1-x}Zn_xFe_2O_4$ spinels [27]. Much larger crystallite sizes have been reported for the $Mg_{1-x}Zn_xFe_2O_4$ [22] and $Zn_{1-x}Cd_xFe_2O_4$ [48] spinels. The estimated values of the microstrains from the D-S and S-S equations do not agree with each other. Values of ε from the D-S method are higher than those from the S-S method. The estimated values of the root-mean-squared strain, ε_{rms} were calculated and shown in Table 4.

Table 4. *The crystallite sizes, strain, Debye-Waller factor and Debye temperatures as a function of x the $Mg_{1-x}Zn_xFeNiO_4$ spinels.*

x	D_{D-S} (nm)	D_{W-H} (nm)	D_{S-S} (nm)	ε x 10^{-3}	ε x 10^{-5}	D.W.F (A^2) using XRD	D.W.F (A^2) using θ_D	θ_D (K) Heat Capacity	θ_D (K) (FTIR)	Avg. θ_D (K) ±1	<u^2> (A^2)
0.0	33	100	61	1.61	1.08	1.0597	0.1723	411	742	577	0.0402
0.2	34	102	70	1.57	1.20	0.9567	0.1551	395	729	562	0.0363
0.4	34	101	77	1.55	1.41	0.8122	0.1129	380	730	555	0.0308
0.6	30	90	74	1.67	2.02	0.7747	0.1190	366	731	549	0.0294
0.8	30	70	39	1.40	1.33	1.1981	0.2270	353	727	540	0.0455
1.0	26	61	34	1.60	1.64	1.4417	0.3032	341	718	530	0.0547
Avg.	31	87	59	1.57	1.45	1.0405	0.1816	393	723	577	0.0395

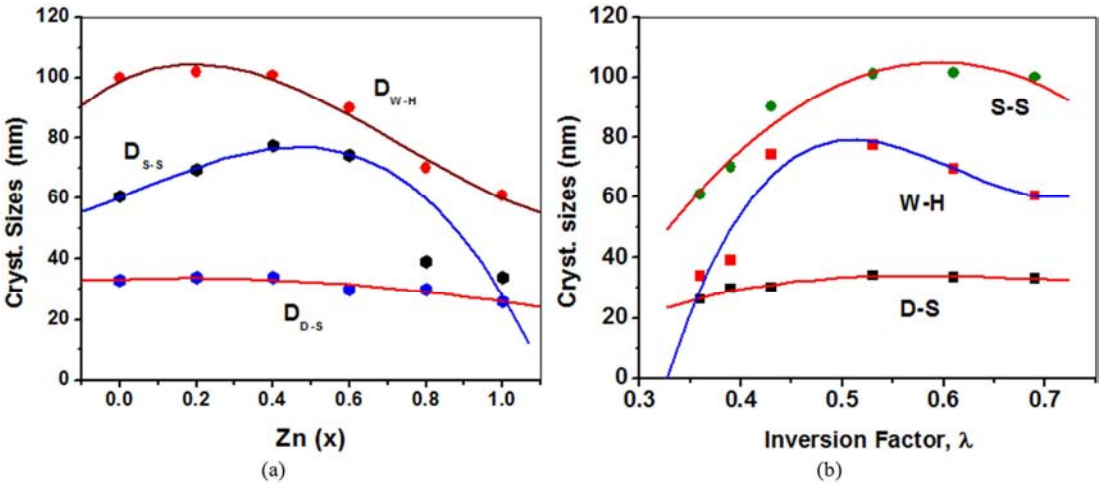

Figure 9. *(a): The crystallite sizes versus the Zn content (x) for the $Mg_{1-x}Zn_xFeNiO_4$ spinels. (b): The crystallite sizes versus the inversion factor λ for the $Mg_{1-x}Zn_xFeNiO_4$ spinels.*

Similar strain results have been reported for ZnO oxide [49, 50] and for other spinels such as the $Ni_{1-x}Zn_xFe_2O_4$ [48]. It has been reported that there is a relation between the inversion factor and the lattice constants [49]. Other studies suggest that there is a relation between the particle sizes and the inversion factor [50, 51]. It was reported that the crystallite sizes decrease as the inversion factor increase in the $Mg_{1-x}Zn_xFeCrO_4$ spinels [22]. The relation between the crystallite sizes and the inversion factor in the $Mg_{1-x}Zn_xFeNiO_4$ spinels has been shown in Figure 9-b. It is clear that the crystallite sizes from the different methods increase first passing through broad maximum then decreases. Comparing Figure 9-a and Figure 9-b conveys that there is some sort of relation between the crystallite sizes and the inversion factors. It appears as a shift of the broad maximum towards the samples of high inversion factors.

3.3. The Order-Disorder in $Mg_{1-x}Zn_xFeNiO_4$ Spinels

The cation distributions in the $Mg_{1-x}Zn_xFeNiO_4$ samples suggest that these samples have the mixed spinel type structure with an inversion factor, λ, in which the Mg^{+2}, Zn^{+2} and Fe^{+3} cations occupy both the A- and B- sites while the Ni^{+3} ions occupy the B- sites and the structural formula can be written as in the following;

$$((Mg^{+2}_{1-x}Zn^{+2}_{x})_{1-\lambda}(Fe^{+3})_{\lambda})_A[(Mg^{+2}_{x}Zn^{+2}_{1-x})_{\lambda}Fe^{+3}_{1-\lambda}Ni^{+3}_{1.0}]_BO_4$$

The Mossbauer investigation reveals the following cation distribution for these spinels [12].

x	Tetrahedral sites	Octahedral sites	λ
0.0	$(Mg^{2+}_{0.31}Fe^{3+}_{0.69})$	$[Mg^{2+}_{0.69}Fe^{3+}_{0.31}Ni^{3+}_{1.00}]$	0.69
0.2	$(Mg^{2+}_{0.19}Zn^{2+}_{0.20}Fe^{3+}_{0.61})$	$[Mg^{2+}_{0.61}Fe^{3+}_{0.39}Ni^{3+}_{1.00}]$	0.61
0.4	$(Mg^{2+}_{0.07}Zn^{2+}_{0.40}Fe^{3+}_{0.53})$	$[Mg^{2+}_{0.53}Fe^{3+}_{0.47}Ni^{3+}_{1.00}]$	0.53
0.6	$(Zn^{2+}_{0.57}Fe^{3+}_{0.43})$	$[Mg^{2+}_{0.40}Zn^{2+}_{0.03}Fe^{3+}_{0.57}Ni^{3+}_{1.00}]$	0.43
0.8	$(Zn^{2+}_{0.61}Fe^{3+}_{0.39})$	$[Mg^{2+}_{0.20}Zn^{2+}_{0.19}Fe^{3+}_{0.61}Ni^{3+}_{1.00}]$	0.39
1.0	$(Zn^{2+}_{0.64}Fe^{3+}_{0.36})$	$[Zn^{2+}_{0.36}Fe^{3+}_{0.64}Ni^{3+}_{1.00}]$	0.36

Table 5. *The inverse factor, order parameter and the configurational entropy in the $Mg_{1-x}Zn_xFeNiO_4$ spinels.*

x	λ	p	2 q	q	4 r	Q	κ	S (J/mol,K)
0.0	0.69	2.69	5.31	2.655	-8.0	-0.035	1.0	15.8606
0.2	0.61	2.61	5.39	2.695	-8.0	0.085	0.91	15.7869
0.4	0.53	2.53	5.47	2.736	-8.0	0.205	0.79	15.3625
0.6	0.43	2.43	5.57	2.785	-8.0	0.355	0.64	14.3361
0.8	0.39	2.39	5.61	2.805	-8.0	0.415	0.58	13.7641
1.0	0.36	2.36	5.64	2.820	-8.0	0.460	0.54	13.2709

The perfect normal, perfect random and perfect inverse configurations have λ=0, 2/3 and 1 respectively. The value λ=2/3 refers to a completely random distributions. As temperature increases the tendency of the normal and inverse spinels increases towards the random, maximum entropy cation distribution at x=2/3. The order parameter Q is related to the inversion factor λ through the following relation [55, 56];

$$Q = 1 - \frac{3\lambda}{2} \qquad (11)$$

Most spinel systems do not show a complete degree of order; they contain some degree of disorder (inversion). The degree of order, Q varies between 1, 0 and -0.5 for the perfectly normal, perfect disorder and perfect inverse respectively. In the perfectly normal order systems all the A^{2+} cations reside at the tetrahedral sites and all the B^{3+} cations reside at the octahedral sites. While for the complete disorder systems 1/3 of the A^{2+} cations and 2/3 of the B^{3+} cations reside at the tetrahedral sites and 2/3 of A^{2+} cations and 1/3 of B^{3+} cations reside at the octahedral sites. Taking the value of the inversion factor 2/3 as a general border to separate the normal from the inverse phase, the current spinels can be classified as "largely normal" for x (0 to 0.6) and "largely inverse" for x (0.6 to 1.0) [56].

In spite of the fact there is no simple generalization between the lattice parameter and the inversion factor. The present partially inverse $Mg_{1-x}Zn_xFeNiO_4$ spinels showed an increase in the lattice parameter a_{exp} from 8.359 Å to 8.409 Å as the inversion factor decreases from 0.69 to about 0.36. Similar results have been reported for the $ZnAl_2O_4$ spinels [57]. The inversion parameter increases in the inverse $MgFe_2O_4$ spinel increases as the pressure increases [58]. Values of the ordering parameter Q for the present spinels have been calculated and presented in Table 5. It is clear that these spinels like the majority of spinels [11] have quite high degree of disorder, κ (=1-Q) and they are too far from being perfect normal or perfect inverse type spinel structure. Table 5 shows that an inverse relation between Q and λ in these spinels. This satisfies the fact that the more inverse the spinel the more the disorder. The order-disorder parameters Q and λ are shown in Figure 10 as a function of Zn content. It is clear that the Q and λ curves cross at about x=0.7. The total randomness corresponds to (Q=0). The sample $MgFeNiO_4$ has almost the complete randomness configuration. Its cation distributions can be written as $(Mg_{1/3}Fe_{2/3})_A[Mg_{2/3}Fe_{1/3}Ni_{3/3}]_BO_4$. The degree of randomness, κ is a reflection of the inversion factor, λ. Both κ and λ decrease as the structure moves towards the spinel structure normality, i.e. as the Zn content (x) increases in the sample. The increasing of cation disorder in spinels is associated with the configurational entropy Sc, [11, 39, 56], which can be written as;

$$Sc = -R\left[\lambda\ln\lambda + (1-\lambda)\ln(1-\lambda) + \lambda\ln\left(\frac{\lambda}{2}\right) + (2-\lambda)\ln\left(1-\frac{\lambda}{2}\right)\right] \quad (12)$$

The configurational entropy for the disorder in spinels systems. It covers the whole range from perfect normal spinel to the perfect inverse spinel through the complete randomness type structure. Values of Sc have been calculate for the whole range from λ=0 to λ=1 and shown plotted in Figure 11. Values of Sc for the present $Mg_{1-x}Zn_xFeNiO_4$ samples have been mapped on the universal curve. It is clear that there is an excellent agreement between the theoretical and calculated values of Sc in the present spinels. Similar Sc results have been reported for the solid solution (Fe_3O_4-Fe_2TiO_4) [60] and $MgGa_2O_4$ spinels [61]. The sample of the complete randomness should have an ordering parameter Q of 0 with an inversion factor λ of 2/3 and has maximum configurational entropy Sc (≈15.861 J/mol,K). The hypothetical samples of perfect normal configuration is going to be the sample $(Mg_{1-x}Zn_x)_A[FeNi]_BO_4$ with Q=1, λ=0, κ=1 and minimum configurational entropy, Sc (=0 J/mol,K). On the other hand the hypothetical sample of perfect inverse configuration is going to be the sample $(Fe)_A[(Mg_{1-x}Zn_x)Ni]_BO_4$ with Q=(-0.5), λ=1, κ=0 with figurational entropy Sc (=2Rln2 ≈11.526 J/mol,K). This equation represents the universal function of the ordering, random, inverse factors and the configurational entropy for the present spinels have been calculated and shown in Table 3. Figure 12 shows Sc as a function of the inverse factor. The Sc increases first then it tends to saturate for λ values higher than 0.5. The inset in Figure 12 shows that the Sc decreases as the Zn content increases in the sample (i.e. as the structure moves towards the normality phase).

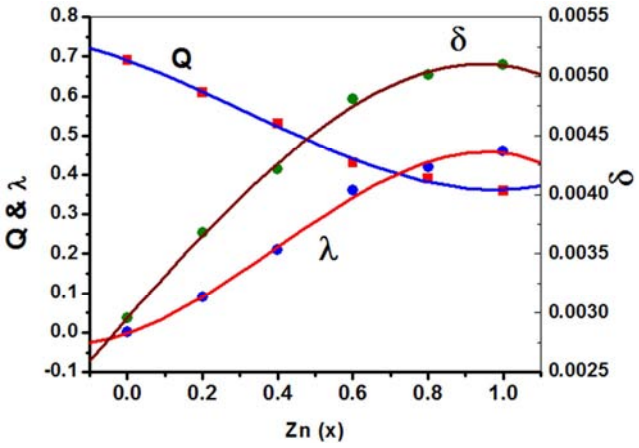

Figure 10. *The ordering parameters Q, λ and δ versus the Zn content (x) for the $Mg_{1-x}Zn_xFeNiO_4$ spinels.*

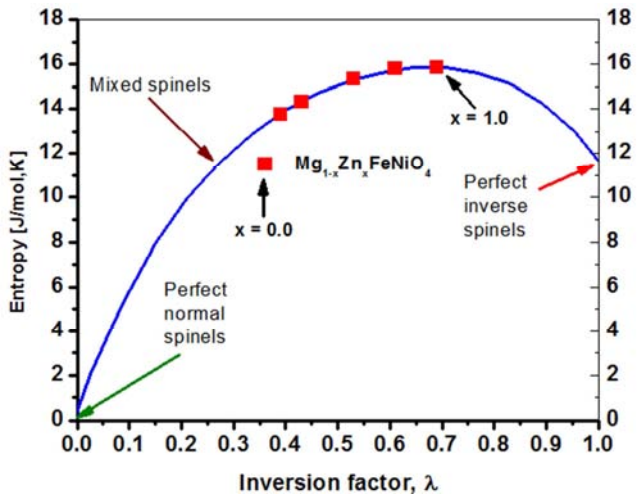

Figure 11. *The universal configurational entropy curve. Values of Sc (red points) for the $Mg_{1-x}Zn_xFeNiO_4$ samples were mapped on the curve.*

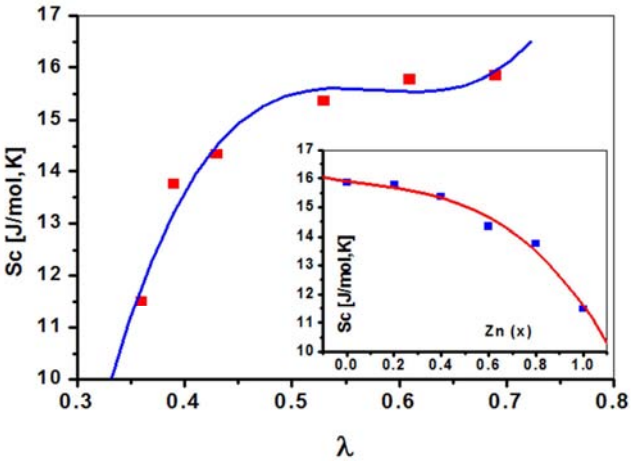

Figure 12. *The configurational entropy, Sc versus the inversion factor, λ. The inset shows the Sc versus for Zn content (x) for the $Mg_{1-x}Zn_xFeNiO_4$ spinels.*

3.4. The Atomic Structure Factor, f

The atomic scattering factor, f, has been defined as the ratio of the amplitude of the scattered waves by an atom to the amplitude of the scattered waves by one electron [13], i.e.;

$$f = \frac{A_{atom}}{A_{elecron}} \tag{13}$$

In order to calculate the structure factor, F for these samples, values of the atomic factor function, f, has to be estimated first. The atomic scattering factor in spinel, f_{tot} consists of participation of the cations at the tetrahedral, f_{tet} and octahedral, f_{oct} sites and the anions, f_{ani} can be written as;

$$\left.\begin{aligned} f_{tet} &= \sum_{i=1}^{n}\left(C_{Mg}f_{Mg} + C_{Zn}f_{Zn} + C_{Fe}f_{Fe}\right) \\ f_{oct} &= \sum_{i=1}^{m}\frac{\left(C_{Mg}f_{Mg}+C_{Zn}f_{Zn}+C_{Fe}f_{Fe}+C_{Ni}f_{Ni}\right)}{2} \\ f_{tot} &= f_{tet} + f_{oct} + 4\,f_{ani} \end{aligned}\right\} \tag{14}$$

where n and m represent the number of cations at the tetrahedral and octahedral sites respectively, while C_i and f_i represent the concentration of the concerned cations and their atomic structural factor respectively. The cations distribution in the $Mg_{1-x}Zn_xFeNiO_4$ spinels reveals that there are only three cations; Mg^{2+}, Zn^{2+} and Fe^{3+} residing at the tetrahedral sites and four cations; Mg^{2+}, Zn^{2+}, Fe^{3+} and Ni^{3+} residing at the octahedral site. Values of f_{atom} for the various atoms as a function of $(\sin(\theta)/\lambda)$ have been tabulated in many X-ray books [13, 23]. It is clear that the ratio, f_{atom}, has its maximum value, which is equal to its atomic number, Z in the forward direction ($2\theta=0^o$) at which the electron scattered waves are totally in phase. As θ increases, the f_{atom} decreases because the scattered waves become increasingly out of phase. Values of f_{atom} are independent of the unit cell size and shape and it decreases as λ increases. However, The resultant effect of both (θ) and (λ) on f_{atom} is that f_{atom} decreases as $(\sin(\theta)/\lambda)$ increases. Values of the atomic factor for the different atoms in each (hkl) planes in the $Mg_{1-x}Zn_xFeNiO_4$ spinels have been calculated and tabulated in Table 6. Values of f_{atom} for the different samples are quite similar. Figure 13-a shows values of f_{atom} for the different atoms in the different (hkl) planes of the samples with x=0.2 as an example. Figure 13-b shows values of f_{tet}, f_{oct}, f_{ani} and f_{tot} for the different (hkl) planes in the $Mg_{1-x}Zn_xFeNiO_4$ spinels. Quite similar results have been reported for the spinels $Mg_{1-x}Zn_xFeCrO_4$ [31].

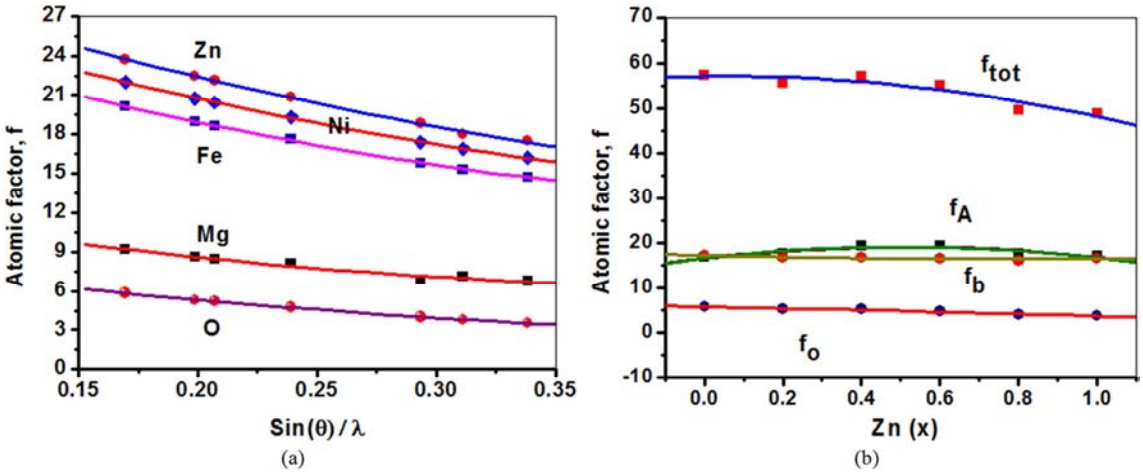

Figure 13. *(a): The atomic function factor for Mg, Zn, Fe, Ni and O atoms versus (sin(θ)/λ) in the $Mg_{1-x}Zn_xFeCrO_4$ spinels. (b): The total atomic function factor for the tetrahedral, f_{tet} octahedral, f_{oct} and f_{Oct} sites as a function of the Zn contents x.*

Table 6. *Atomic function factor of the different atoms as a function of x and sin(θ)/λ for the $Mg_{1-x}Zn_xFeNiO_4$ spinels.*

	X = 0.0					
Sin(θ)/λ	(hkl)	Mg	Zn	Fe	Ni	O
0.169505	220	9.17941	23.74179	20.18080	22.01130	5.84089
0.198738	311	8.62398	22.45552	18.95300	20.75426	5.30227
0.207049	222	8.44707	22.13214	18.66739	18.23289	5.20132
0.239086	400	8.07467	20.91472	17.61015	17.42386	4.75279
0.293451	422	6.82443	18.84886	15.81612	17.42922	3.99169

	X = 0.0					
0.311242	511	7.10386	18.00710	15.34144	16.90772	3.78758
0.338345	440	6.75151	17.52633	14.71806	16.20302	3.51655
	X = 0.2					
Sin(θ)/λ	(hkl)	Mg	Zn	Fe	Ni	O
0.169083	220	9.18742	23.76033	20.19850	22.02942	5.84165
0.198289	311	8.63250	22.47527	18.97185	20.77356	5.30227
0.206651	222	8.47363	22.14726	18.68052	20.46727	5.20689
0.238675	400	8.07789	20.93036	17.68973	19.34638	4.75855
0.292909	422	6.83474	18.86948	15.83402	17.44820	3.99928
0.310675	511	7.11122	18.14988	15.02326	16.89645	3.79325
0.337806	440	6.75852	17.54143	14.79946	16.21704	3.52194
	X = 0.4					
Sin(θ)/λ	(hkl)	Mg	Zn	Fe	Ni	O
0.169201	220	9.18517	23.75514	20.19354	22.02434	5.84144
0.198337	311	8.63161	22.47318	18.96985	20.77151	5.30299
0.207006	222	8.46689	22.13422	18.66919	20.48980	5.21592
0.238881	400	8.07510	20.92250	17.61691	19.33915	4.75566
0.292754	422	6.83767	18.87534	15.83911	17.45361	4.00145
0.310442	511	7.11425	18.20853	15.07143	16.90250	3.79558
0.337764	440	6.75907	17.54261	14.80043	16.21814	3.52236
	X = 0.6					
Sin(θ)/λ	(hkl)	Mg	Zn	Fe	Ni	O
0.169007	220	9.18887	23.72437	20.20170	22.03269	5.84179
0.198150	311	8.63160	22.48140	18.97770	20.77955	5.30333
0.206129	222	8.48356	22.16711	18.69776	18.55498	5.21430
0.238014	400	8.08681	20.95545	17.64553	17.68647	4.76780
0.292542	422	6.84171	18.88341	15.84612	17.46103	4.00441
0.310250	511	7.11675	18.25696	15.31822	16.93350	3.79750
0.336839	440	6.77120	17.57061	14.75271	16.24220	3.53161
	X = 0.8					
Sin(θ)/λ	(hkl)	Mg	Zn	Fe	Ni	O
0.168887	220	9.19114	23.76897	20.16474	22.03785	5.84200
0.198003	311	8.63794	22.48786	18.98386	20.78586	5.30359
0.205693	222	8.49184	22.18367	18.71214	18.70751	5.22030
0.237515	400	8.09354	20.97441	17.66199	17.80871	4.77478
0.292265	422	6.84696	18.89391	15.85524	17.47071	4.00828
0.310032	511	7.11959	18.31199	15.36342	16.93917	3.79968
0.336244	440	6.77882	17.58516	14.76638	16.25765	3.53756
	X = 1.0					
Sin(θ)/λ	(hkl)	Mg	Zn	Fe	Ni	O
0.169505	220	9.19114	23.77362	20.21119	22.04241	5.84501
0.198738	311	8.64003	22.49269	18.98848	20.74584	5.30379
0.207049	222	8.49457	22.18913	18.71688	20.50075	5.22231
0.239086	400	8.09553	20.98001	17.66685	19.38696	4.77684
0.293451	422	6.84479	18.88958	15.85148	17.46672	4.00669
0.311242	511	6.99208	18.32447	16.94415	16.94415	3.70160
0.338345	440	6.78206	17.59212	14.77210	16.26411	3.54004

3.5. The Structure Factor, F_{hkl}

The scattered waves by the individual atoms can be represented by the structure factor F, which can be written as;

$$F_{hkl} = \sum_1^N f_{atom}\, e^{2\pi i\,(h\,u_n + k\,v_n + l\,w_n)} \quad (15)$$

Where f_{atom} represents the atomic scattering factor of the n^{th} atom and N represents the total number of atoms in the unit cell each with fractional coordinates u_n, v_n and w_n. The u_n, v_n and w_n coordinates for the face centered cubic (FCC) structure as in spinels reduce to the four numbers (0,0,0), (0,1/2,1/2), (1/2,0,1/2) and (1/2,1/2,1/2). This leads to quite simple expression for F_{hkl} due to the following reasons; First when values of h, k and l are all even or all odd (unmixed) the value of $F_{hkl} = 4f_{atom}$. Second when values of h, k and l are a combination of odd and even (mixed) the F_{hkl} will be equals to 0. Then;

$$\left.\begin{array}{c} F_{hkl} = 4\, f_{\text{atom}}\ (hkl\ are\ all\ even\ or\ all\ odd \\ -unmixed) \\ F_{hkl} = 0\ \left(\begin{array}{c} hkl\ are\ combination\ of odd\ and\ even \\ -mixed \end{array}\right) \end{array}\right\} \quad (16)$$

The structure factors of the FCC planes have been calculated using the following relations, which takes into account the small effects of the oxygen positional parameter, u [10-57];

$$\left.\begin{aligned} F_{111} &= 4\sqrt{2}F_A - 8F_B + 16\sqrt{2}F_O\left(cos^3(2\pi u) + sin^3(2\pi u)\right) \\ F_{220} &= 8f_A + 32f_O\, cos^2(4\pi u) \\ F_{311} &= 4\sqrt{2}f_A + 8f_B + 16\sqrt{2}f_O\left(cos^2(2\pi u)\cos(6\pi u) - sin^2(2\pi u)\sin(6\pi u)\right) \\ F_{222} &= 16f_B + 32f_O\, sin^3(4\pi u) \\ F_{333} &= 4\sqrt{2}F_A + 8F_B + 16\sqrt{2}F_O\left(cos^3(6\pi u) - sin^3(6\pi u)\right) \\ F_{400} &= 8f_A - 16f_B + 32f_O\, cos(8\pi u) \\ F_{422} &= 8f_A + 32f_O\, cos(8\pi u)\, cos^2(4\pi u) \\ F_{511} &= 4\sqrt{2}f_A + 8f_B + 16\sqrt{2}f_O\left(cos^2(2\pi u)\cos(10\pi u) - sin^2(2\pi u)\sin(10\pi u)\right) \\ F_{440} &= 8f_A + 16f_B + 32f_O\, cos^2(8\pi u) \end{aligned}\right\} \quad (17)$$

Values of the structure factors, F_{hkl} for the different (hkl) planes are shown in Table 7.

Table 7. *Values of the structure factors of the different (hkl) planes and of the tetrahedral, octahedral and onion sites as a function of the Zn contents and the oxygen positional factor* $u_{avg.}$

x	u_{avg}	FA	FB	FO	F220	F311	F222	F400	F422	F511	F440
0.0	0.3780	67.0815	69.2023	23.3636	-535.479	925.6678	361.3603	-1315.870	535.4831	984.7769	2386.840
0.2	0.3787	70.7640	66.8131	21.2091	-564.522	926.5642	392.7017	-1178.410	564.5298	992.0778	2307.470
0.4	0.3792	77.3515	62.9670	20.8053	-616.822	932.1586	344.6864	-1050.450	616.8338	1004.7083	2284.117
0.6	0.3798	77.9750	62.6379	19.0112	-621.447	932.6773	397.3761	-982.056	621.4648	1008.0269	2224.986
0.8	0.3800	70.6644	64.0464	15.9668	-563.176	903.7879	517.0129	-966.085	563.1935	969.6004	2092.472
1.0	0.3801	68.1899	66.4176	15.1503	-543.409	909.0293	581.0315	-997.754	543.4277	972.6756	2084.610

3.6. Debye-Waller Factor (DWF)

The thermal vibrations of atoms about their positions attenuate the X-ray diffracted intensities. A correction for these disruptions can be achieved by employing the Debye-Waller factor (DWF) or the temperature factor [13]. The intensity of the diffracted X-ray spectra from the powder samples is related to the Debye-Waller factor, B_T through the following relations [64]:

$$\left.\begin{aligned} I_{cal} &= K\, I_{obs} \exp\left(\frac{-2B_T sin^2(\theta)}{\lambda^2}\right) \\ Ln\left(\frac{I_{cal}}{I_{obs}}\right) &= \ln(K) + B_T\left(\frac{-2\, sin^2(\theta)}{\lambda^2}\right) \end{aligned}\right\} \quad (18)$$

Where I_{cal} and I_{obs} represent the calculated and observed intensities respectively and K represents the scale factor. The DWF can be estimated from the least square fittings of the $\ln(I_{cal}/I_{obs})$ versus $(-2\sin^2(\theta)/\lambda^2)$ of the X-ray intensities of the concerned (hkl) planes. The I_{cal}(hkl) have been estimated employing the following relation [13, 23];

$$I_{cal} = |F|^2.(MF).(LP).(AF).(TF) \quad (19)$$

where F, MF, LP, AF and TF represent the structure factor, the multiplicity factor, Lorentz-Polarization factor, absorption factor and temperature factor respectively. The absorption (AF) and temperature (TF) factors vary in opposite directions with temperature and they were usually omitted especially for the problems where relative intensity calculations are concerned [23-26]. Therefore, equation (16) will be reduced to the following simple approximate form:

$$I_{hkl} = |F_{hkl}|^2.(MF).(LP) \quad (20)$$

The most sensitive planes to the cation distributions at the tetrahedral sites are the planes (220), (422) and (440), while the (400) and (440) planes are the most sensitive for cations on both the tetrahedral and octahedral sites. The (311) planes are nearly independent of the anions. The intensities I_{220}, I_{311}, I_{222}, I_{400}, I_{422}, I_{511} and I_{440} were calculated using equation (17). The calculated and observed relative results were obtained by normalizing with respect to the most intensive reflection I_{311}, which has been taken as 100%. The ratios of the calculated to the observed relative intensities (I_c/I_o) are shown in Figure 14-a as a function of Zn content in the sample. It is clear that the relative intensities vary nonlinearly with different manners with Zn contents. Moreover, as the peak areas are much more reliable than peak heights as a measure of peak intensity, values of the relative integrated areas under the peak (A_{obs}/A_{311}) have been calculated and presented in Table 8 as a function of Zn content. Figure 14-b shows that the relative areas increase almost linearly with x. It means that the presence of Zn in the sample enhances the area of the (hkl) reflections. The estimation of both I_{cal} and I_{obs} allows for the calculation of the Debye Waller factor, B_T for the present $Mg_{1-x}Zn_xFeNiO_4$ spinels using equations (15). This can be achieved by plotting $\ln(I_c/I_o)$ versus $(-2\sin^2(\theta)/\lambda^2)$ for all the (hkl) planes for each sample. The slope will be equals to B_T for that sample. Values of B_T for the present $Mg_{1-x}Zn_xFeNiO_4$ spinels are shown in Table 2. It is clear that they lie in the range (0.77–1.44A^2). These values are in good agreement with those reported for other spinels such as $ZnFe_{1-x}Cr_xO_4$ (0.829–1.234A^2)| [22], $CuFe_{2-x}Al_xO_4$ (0.489–1.390A^2) [65] and $ZnFe_2O_4$ (0.872A^2) [66]. Moreover, it is clear that values of B_T for the $Mg_{1-x}Zn_xFeNiO_4$ spinels fall in two separate regions as shown in Figure 15 the first region is for the x values (0.0–0.6) and the second region is in the range (0.6–1.0). Values of the Debye Waller factors vary nonlinearly with the Zn content. The inset in

Figure 15 shows DWF values versus the microstrain in these spinels. The extrapolation of this relation to zero value of ε gives the effective DWF for these samples, which equals to 0.513A^2. A value of 0.896A^2 has been reported for the normal $ZnFe_{2-x}Cr_xO_4$ spinels [22]. The relation between the Debye Waller factor and the crystallite sizes has been shown in Figure 16. This figure shows that both D and DWF decrease as x increases in the region of the "largely normal" spinels while they behaves quite differently in the region of the "largely inverse" spinels. The behaviours of the DWF with the oxygen parameter, u is quite similar to the relation between D and DWF.

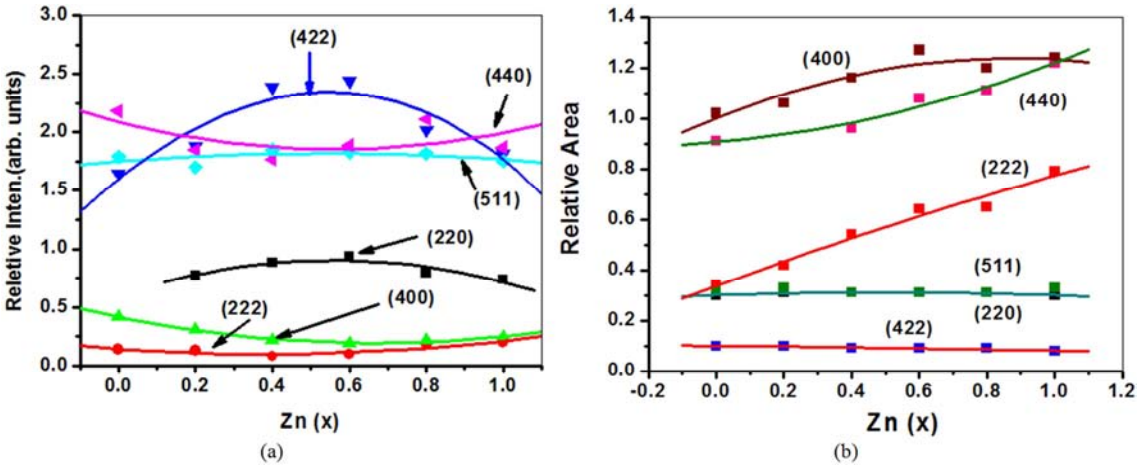

Figure 14. *(a): The relative intensity of the (hkl) reflections as a function of Zn content (x). (b): The relative areas under the (hkl) reflections as a function of Zn content (x) for $Mg_{1-x}Zn_xFeNiO_4$ spinels.*

Table 8. *Relative diffracted intensities and relative areas of the different (hkl) planes for the $Mg_{1-x}Zn_xFeNiO_4$ spinels.*

Relative Intensities (I_{obs}/I_{311})						
x	**(220)**	**(222)**	**(400)**	**(422)**	**(511)**	**(440)**
0.0	2.19	0.14	0.42	1.65	1.79	2.18
0.2	0.77	0.13	0.31	1.88	1.70	1.85
0.4	0.88	0.08	0.22	2.39	1.85	1.77
0.6	0.94	0.10	0.19	2.44	1.83	1.89
0.8	0.79	0.18	0.22	2.02	1.82	2.11
1.0	0.74	0.20	0.24	1.82	1.75	1.87

Relative Areas (A_{obs}/A_{311})						
x	**(220)**	**(222)**	**(400)**	**(422)**	**(511)**	**(440)**
0.0	0.30	0.34	1.02	0.10	0.32	0.91
0.2	0.31	0.42	1.06	0.10	0.33	0.33
0.4	0.31	0.54	1.16	0.09	0.31	0.96
0.6	0.31	0.64	1.27	0.09	0.31	1.08
0.8	0.31	0.65	1.20	0.09	0.31	1.11
1.0	0.30	0.79	1.24	0.08	0.33	1.22

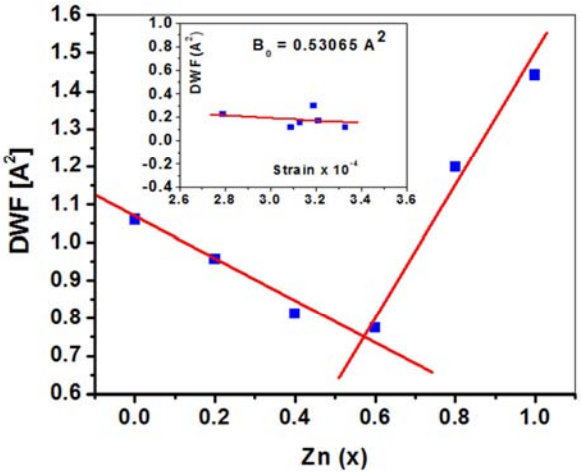

Figure 15. *The Debye-Waller factor (DWF) versus Zn content (x). The inset shows the DWF versus strain for the $Mg_{1-x}Zn_xFeNiO_4$ spinels.*

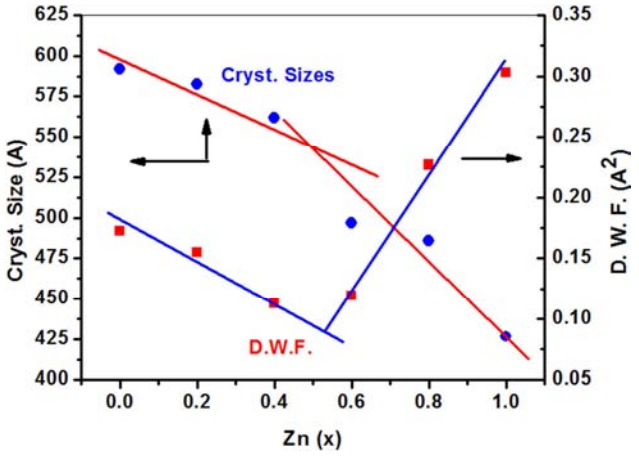

Figure 16. *The crystallite sizes and DWF versus the versus the Zn content (x) for the $Mg_{1-x}Zn_xFeNiO_4$ spinels.*

3.7. The Effective Debye Temperature, θ_D

An important parameter of the thermal properties and heat capacity in particular the effective Debye temperature, θ_D, which is related to the Debye-Waller factor B_T and can be roughly estimated using the following relations [13];

$$\left.\begin{aligned} \theta_D &= \left(\frac{6h^2 N_A T}{MK_B B_T} W(y)\right)^{\frac{1}{2}} \\ W(y) &= \left(\phi(y) + \frac{y}{4}\right) \\ y &= \frac{\theta_D}{T} \end{aligned}\right\} \quad (21)$$

This equation can be simplified to have the following form at T=300 K;

$$B_T = \frac{1.15\,x10^4}{M} x \frac{300}{\theta_D^2} x \left(\phi(y) + \frac{y}{4}\right) \quad (22)$$

where B_T, $\phi(y)$, K_B, h, T and M represent Debye-Waller factor, Debye function, Boltzmann's constant, Plank's constant, absolute temperature and molecular mass of the $Mg_{1-x}Zn_xFeNiO_4$ spinels. Values of the ϕ (y) function can be found in standard tables [67]. It is clear that the calculations of B_T require the estimation of the Debye temperature θ_D. Values of the Debye temperatures for the present $Mg_{1-x}Zn_xFeNiO_4$ spinels can be estimated using known values of θ_D for similar $Mg_{1-x}Zn_xFeCrO_4$ spinels [68] using scaling law, which relates Debye temperatures of the closely related compounds to their molecular masses as in the following relations [69];

$$\left.\begin{aligned} \frac{\theta_{D(Mg_{1-x}Zn_xFeNiO_4)}}{\theta_{D(Mg_{1-x}Zn_xFeCrO_4)}} &= \left(\frac{M_{Mg_{1-x}Zn_xFeCrO_4}}{M_{Mg_{1-x}Zn_xFeNiO_4}}\right)^{\frac{1}{2}} \\ \theta_{D(Mg_{1-x}Zn_xFeNiO_4)} &= \theta_{D(Mg_{1-x}Zn_xFeCrO_4)} \left(\frac{M_{Mg_{1-x}Zn_xFeCrO_4}}{M_{Mg_{1-x}Zn_xFeNiO_4}}\right)^{\frac{1}{2}} \end{aligned}\right\} \quad (23)$$

The calculated values of θ_D for the $Mg_{1-x}Zn_xFeNiO_4$ spinels are shown in Table 4 together with θ_D from the FTIR relation. Figure 17-a shows that values of θ_D decrease as the Zn^{2+} contents increase in the sample. This might be caused by the enhancements of the lattice vibrations, which causes reduction in the values of the Debye temperatures, another reason might be the increase of the average molecular mass, which has an inverse relation with θ_D. Values of θ_D are in the range (321–378 K) compare well with those reported for other spinels such as $ZnFe_{2-x}Cr_xO_4$ (284–355 K) [22] $CuFe_{2-x}Al_xO_4$ (282–472 K) [65] $Ni_{0.5}Zn_{0.5}Fe_2O_4$ (260–330 K) [70] and $NiFe_{2-x}Cr_xO_4$ (650–675K) [41]. The substitution of the θ_D values in the equations allows for the estimation of the DWF for these spinels. The average values of the Debye temperature have been plotted versus the average force constants, K_{avg} in Figure 17-b. This figure shows clearly the inverse relation between θ_D and K_{avg}. Knowing values of the effective Debye temperatures and the function W(y) allows for the calculation of the effective Debye Waller factor B_T and the temperature factor (M_T).

Table 9. *Debye temperature, the function, Debye-Waller factor, Temperature factor as a function of x and sin(θ)/λ for the $Mg_{1-x}Zn_xFeNiO_4$ spinels.*

x	θ_D(K) average	Y= θ_D/300	ϕ(y)	y/4	B_T	sin(θ)/λ	(sin(θ)/λ)^2	M_T	exp(-2M_T)
0.0	577	1.9217	0.6185	0.4804	0.05624	0.169063	0.028582	0.00161	0.99679
0.2	562	1.8733	0.6260	0.4683	0.05664	0.198213	0.039289	0.00223	0.99556
0.4	555	1.8500	0.6295	0.4625	0.05578	0.206480	0.042634	0.00238	0.99526
0.6	549	1.8283	0.6328	0.4571	0.05494	0.238428	0.056848	0.00312	0.99377
0.8	540	1.8000	0.6370	0.4500	0.05456	0.292640	0.085638	0.00467	0.99070
1.0	530	1.7650	0.6426	0.4413	0.05468	0.310421	0.096361	0.00527	0.98952

Table 9 shows values of the concerned parameters; B_T, y, ϕ(y), M, θ_D and M_T. It is clear that values of B_T using Debye temperatures are lower than those obtained using the integrated intensities of the scattered Bragg XRD reflections. This might be caused by the high values of Debye temperatures θ_D, which have an inverse relation with the Debye Walle factors. The temperature factor (M_T) is related to the effective Debye-Waller factor (B_T) through the following relation [13];

$$\left.\begin{aligned} e^{-2M_T} &= e^{-2B_T\left(\frac{\sin\theta}{\lambda}\right)^2} \\ M_T &= B_T\left(\frac{\sin\theta}{\lambda}\right)^2 \end{aligned}\right\} \quad (24)$$

The temperature factors of these samples have been calculated and shown in Table 9. Figure 18 shows the temperature factor as a function of (sin(θ)/λ) for the sample with x=0.4 as an example. It is clear that values of M_T decrease as the (sin(θ)/λ) increases. Similar results have been shown by the Cr metal [13] and $ZnFe_{2-x}Cr_xO_4$ spinel [22]. Moreover, Debye temperature θ_D is related to the average infrared primary bands frequency υ_{avg} through the following relations [71, 72];

$$\left.\begin{aligned} \theta_D &= \frac{h\,c\,v_{avg}}{K_B} \\ \theta_D &= 1.439\,v_{avg} \end{aligned}\right\} \quad (25)$$

where c, h and K_B represent the velocity of light in cm/s, Plank's constant and Boltzmann constant respectively. The Debye temperatures of the $Mg_{1-x}Zn_xFeNiO_4$ spinels can be calculated using equation (22). The calculated values of θ_D are shown in Table 4. The relation between θ_D and the

average force constant K_{avg} is shown in Figure 18. It is clear that there are two separate regions in these spinels. Values of θ_D from the heat capacity scaling and infrared spectroscopy are not the same. Similar results have been reported for other spinels. It has been well established that values of Debye temperatures obtained from different experimental measurements such as elastic constant, heat capacity and infrared spectroscopy are generally in differences [46].

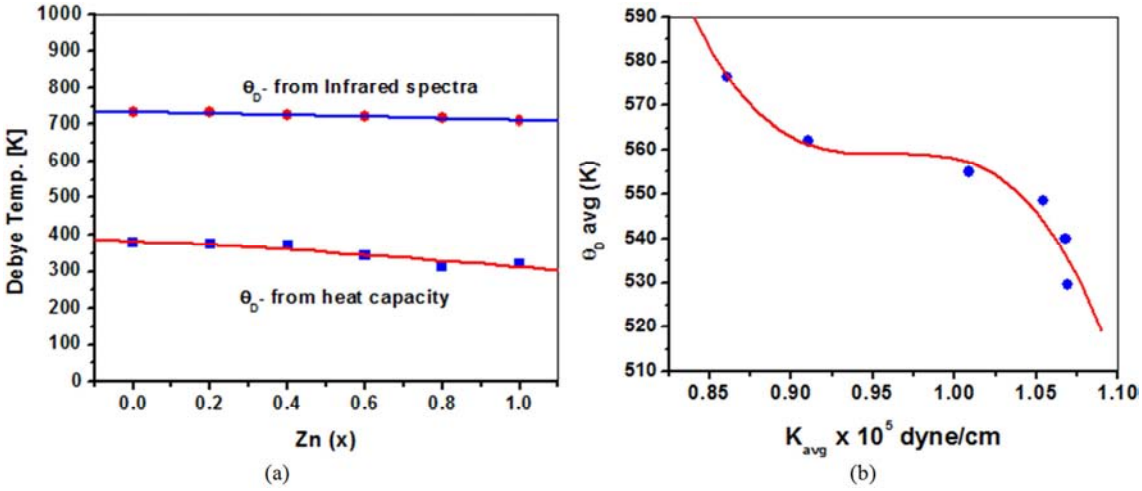

Figure 17. *(a): Debye temperatures versus the Zn content (x) for the $Mg_{1-x}Zn_xFeNiO_4$ spinels. (b): The effective Debye temperatures versus the average force constant K_{avg} in the $Mg_{1-x}Zn_xFeNiO_4$ spinels.*

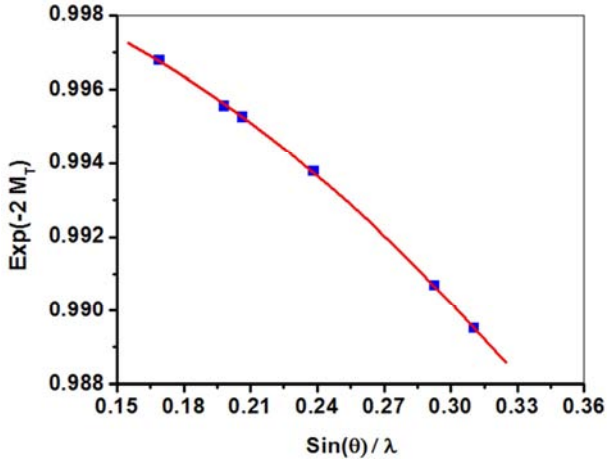

Figure 18. *The temperature factor versus the Zn content (x) for the $Mg_{1-x}Zn_xFeNiO_4$ spinels.*

3.8. The FT-IR Analysis

The infrared (FT-IR) transmission spectra of the $Mg_{1-x}Zn_xFeNiO_4$ spinels are shown in Figure 19-a. The main distinctive features of these spectra are the two dominant metal–oxygen absorption bands at ν_1 and ν_2. These bands appear in the IR spectra of most spinels [73]. Values of ν_1 and ν_2 for the $Mg_{1-x}Zn_xFeNiO_4$ spinels fall in the range (600–570 cm^{-1}) and (420–430 cm^{-1}) respectively. These bands are caused by the intrinsic valence vibrations of the metal cations at the tetrahedral and octahedral sites, M_{tet}–O and M_{oct}–O respectively. Values of ν_1 and ν_2 shift to lower values as the Zn content increases. Similar results have been reported for the spinels $Mg_{1-x}Zn_xFe_2O_4$ [21] and $Cu_{1-x}Zn_xFe_2O_4$ [33]. This is an indication of the weakening of the cation-anion bonds at the tetrahedral and octahedral sites. The replacement of the Mg with Zn causes redistributions of the cations at the A and B sites. This might be linked with the variations of the average cation radii at the A- and B-sites. It is clear that both r_A and r_B increase with x. Values of the band positions ν_1 and ν_2 are listed in Table 10 as a function of Zn content. The absorption bands ν_1 and ν_2 correspond to the stretching vibrations of the Mg^{2+}–O^{-2}, Zn^{+2}–O^{-2}, Fe^{3+}–O^{-2} and Ni^{+3}–O^{-2} bonds at the tetrahedral and octahedral sites. There are many factors responsible for the differences in position of the two bands such as differences in the average metal-oxygen distances, electronegativity, ionic radii and the force constants at the A- and B- sites. Similar results have been reported for the $Mg_{1-x}Zn_xFeCrO_4$ [31-34] and $NiFe_{2-x}Cr_xO_4$ [39-42] spinels. But they are differing from those of the $ZnFe_{2-x}Cr_xO_4$ [22-25] and $MgFe_{2-x}Cr_xO_4$ [24-27] spinels, in which the values of the bands ν_1 and ν_2 shift to higher values (increase) with the Cr content. Figure 19-b shows details of the other absorption bands. The bands at 1638 and 2730 cm^{-1} correspond to other O–H group confirming the presence of interlayer water and the oscillations of the H–O–H bonds and they are independent of the sample compositions. These bands might be assigned to the formation of hydrogen bonds between the hydroxyl groups, which might be caused by the water absorption by the samples during the compaction of the sample powders with KBr as pellets. The wide absorption band appeared at (3450−3470 cm^{-1}) corresponds to O–H bond stretching vibrations of H_2O present in the interlayer space. Similar results have been reported for most of the spinels such as the Co-Zn ferrites [28].

Table 10. *The absorption bands, molecular weight and force constants at the tetrahedral and octahedral sites of the $Mg_{1-x}Zn_xFeNiO_4$ spinels.*

x	v1	v2	vavg	M1	M2	Kt	Ko	Kavg	Kt/Ko
0.0	600	431	515.5	46.0676	46.3879	126373	45757	86065	2.7619
0.2	588	425	506.5	51.7594	47.6495	136364	45702	91033	2.9838
0.4	598	417	507.5	57.4512	48.9111	156551	45162	100857	3.4664
0.6	587	429	508.0	61.2800	51.1042	160898	49942	105420	3.2217
0.8	585	425	505.0	61.6614	55.0210	160798	52772	106785	3.0470
1.0	581	417	499.0	61.9474	58.9855	159342	54464	106903	2.9256

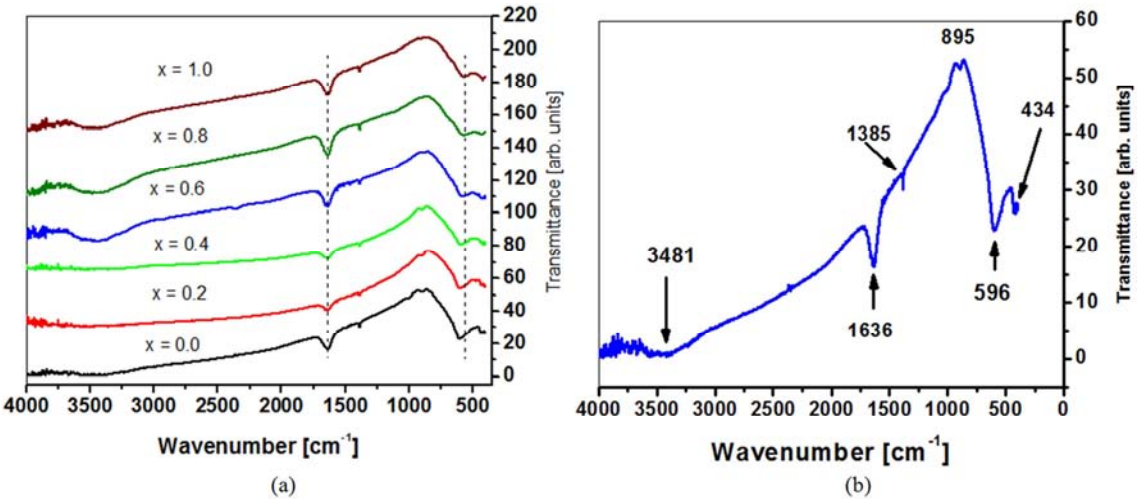

Figure 19. *(a): The FTIR spectra for the samples of the $Mg_{1-x}Zn_xFeNiO_4$ spinels in the range (400-4000) cm^{-1}. (b): the IR spectra showing details of the absorption bands of the $Mg_{1-x}Zn_xFeNiO_4$ spinels.*

The force constants K_t and K_o at the tetrahedral and octahedral sites respectively have been calculated using the following equations [73]:

$$\left.\begin{aligned} K_t &= 7.62\ M_1 \nu_1^2\ 10^{-3} \left(\frac{\text{dyne}}{\text{cm}}\right) \\ K_o &= 10.62 \left(\frac{M_2}{2}\right) \nu_2^2\ 10^{-3} \left(\frac{\text{dyne}}{\text{cm}}\right) \end{aligned}\right\} \qquad (26)$$

where M_1 and M_2 are the average molecular mass of the cations at the tetrahedral and octahedral sites respectively. Values of the force constants K_t and K_o have been listed in Table 10 as a function of Zn^{2+} content. It is clear that values of K_t and K_o increase as Zn content increases. It is clear that values of K_t are higher than those for K_o by more than 3 times. This difference can be attributed to the differences in band stretching between ν_1 and ν_2 bands. The high force constants have been attributed to the band stretching at the tetrahedral sites rather than that at the octahedral sites [74]. The force constants at the tetrahedral and octahedral sites increase in spite of the increases in the bond length at the two sites. These behaviors have been attributed to the oxygen ability in forming strong bonds with cations even at larger bond lengths [75]. Moreover, the force constants in spinels are largely influenced by the nature of the cation distributions. Since these spinels are mixed spinels it is hard to establish the normal direct relationships between the bond lengths and the force constants because the other factors such as the molecular mass, bond lengths, electronegativity and the ionic radii were left free to change and not fixed. The average values of the force constants, K_{avg}, electronegativities, χ_{avg} and bond lengths, R_{avg} increase as the Zn content increase in the $Mg_{1-x}Zn_xFeNiO_4$ spinels as shown in Figure 20.

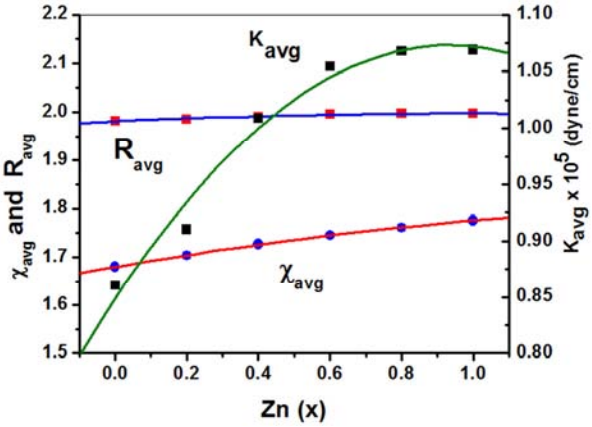

Figure 20. *The average values of the force constants, electronegativities and bond lengths in the $Mg_{1-x}Zn_xFeNiO_4$ spinels.*

3.9. The Electronegativity, χ

The electronegativity describes the tendency of an atom to attract the charge density towards itself. The Pauling electronegativity difference $\Delta\chi$ provides measure of the cationic bond strength and its variations reflect the bond length changes. The electronegativity differences $\Delta\chi$ can be estimated at the tetrahedral χ_A and octahedral χ_B sites of spinels using the following relations [22, 76];

$$\left.\begin{aligned} \chi_A &= (C^A_{Mg^{2+}})(\chi_{Mg^{2+}}) + (C^A_{Zn^{2+}})(\chi_{Zn^{2+}}) + (C^A_{Fe^{3+}})(\chi_{Fe^{3+}}) \\ \chi_B &= \frac{(C^B_{Mg^{2+}})(\chi_{Mg^{2+}})+(C^B_{Zn^{2+}})(\chi_{Zn^{2+}})+(C^B_{Fe^{3+}})(\chi_{Fe^{3+}})+(C^B_{Ni^{3+}})(\chi_{Ni^{3+}})}{2} \\ \Delta\chi_A &= \chi_O - \frac{\chi_A}{4} \text{ and } \Delta\chi_B = \chi_O - \frac{\chi_B}{6} \end{aligned}\right\} \quad (27)$$

where χ_A and χ_B represent the Pauling electronegativities of the cations at the tetrahedral and octahedral sites respectively. Values of the Pauling electronegativity for the Mg^{2+}, where χ_A and χ_B represent the Pauling electronegativities of the cations at the tetrahedral and octahedral sites respectively. Values of the Pauling electronegativity for the Mg^{2+}, Zn^{2+}, Fe^{3+} and Ni^{3+} ions have been taken as 1.31, 1.65, 1.83 and 1.91 respectively and 3.44 for the oxygen. The calculated values of χ_A, χ_B, $\Delta\chi_A$ and $\Delta\chi_B$ are shown in Table 11.

Table 11. *The electronegativities and force constants at the tetrahedral and octahedral sites in the $Mg_{1-x}Zn_xFeNiO_4$ spinels.*

x	χA	χB	χavg	ΔχA	ΔχB	KAA	KAB	KBB	KAB/KBB
0.0	1.6688	1.6906	1.6797	3.0228	3.1582	2.7849	2.8213	2.8588	0.9871
0.2	1.6952	1.7114	1.7033	3.0162	3.1548	2.8737	2.9012	2.9289	0.9905
0.4	1.7216	1.7322	1.7269	3.0096	3.1513	2.9639	2.9822	3.0005	0.9939
0.6	1.7274	1.7633	1.7454	3.0082	3.1461	2.9839	3.0459	3.1092	0.9796
0.8	1.7202	1.8009	1.7606	3.0010	3.1399	2.9591	3.0979	3.2432	0.9552
1.0	1.7148	1.8376	1.7762	3.0113	3.1337	2.9405	3.1511	3.3768	0.9332

Figure 21 shows that the electronegativities at the A- and B- sites behave differently as the Zn content increase. The migration of Zn^{2+} cations from A- sites to the B- sites contributes negatively to χ_A and positively to χ_B. The values of χ_A passing through maxima centered at about x=0.6, while χ_B kept increasing as x increases.

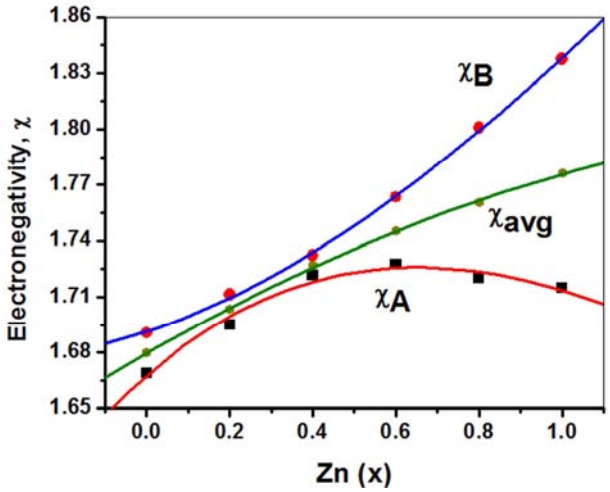

Figure 21. *The electronegativities at the tetrahedral and octahedral sites of the $Mg_{1-x}Zn_xFeNiO_4$ spinels.*

The bond stretching forces K_{AB} in spinels between the cations at the tetrahedral and octahedral sites has been defined as a function of the electronegativities of these cations as in the following equation [39, 77];

$$K_{AB} = aN\left(\frac{\chi_A \chi_B}{r_e^2}\right)^{\frac{3}{4}} + b \quad (28)$$

where a and b are constants, N is the bond order and r_e is the equilibrium distance. This expression has been simplified by assuming that a, N and r_e values are approximately constant, while b is small and can be neglected. These simplifications results in quite simple expression for the force constant K_{AB} as in the following simple forms [39];

$$\left.\begin{aligned} K_{AA} &= \chi_A \chi_A \\ K_{AB} &= \chi_A \chi_B \\ K_{BB} &= \chi_B \chi_B \end{aligned}\right\} \quad (29)$$

The bond forces K_{AA}, K_{AB} and K_{BB} have been considered as a qualitative measure of the repulsive (or attractive) forces between A-A, A-B and B-B cations respectively. It has been argued that the spinel structure will be preferred for small K_{AB}/K_{BB} ratio. Values of K_{AA}, K_{AB}, K_{BB} and the ratio K_{AB}/K_{BB} have been calculated for the $Mg_{1-x}Zn_xFeNiO_4$ spinels and presented in Table 11. Values of the K_{AB}/K_{BB} ratio is less than 1 satisfying the argument. Moreover, the relation between the bonds forces K_{AB} and the ionic radii ratio r_A/r_B has been plotted for large number of spinels and other compounds [39]. This relation has been reshown in Figure 22. The calculated values of K_{AB}(≈0.22) and the ratio r_{ab}/r_{ib}(≈1.01) for the present spinels $Mg_{1-x}Zn_xFeNiO_4$ have been mapped on this Figure The symbol "X" indicates the location of present spinels among others on this plot. It clear that it lies in the inverse spinel region. Moreover mapping values of K_{AB}(≈0.22) against the ratios r_A/r_O(≈0.51) and r_B/r_O(≈0.50) on the three dimensional surface plot (Figure 3 in ref. [39]) proves that the present $Mg_{1-x}Zn_xFeNiO_4$ samples have the spinel type structure. It has also been argued that the radius ratio plays the dominant role in determining the spinel structure. The radius ratios for large number of spinels fall within the following limits; (r_A/r_O= 0.36–0.65) and (r_B/r_O= 0.35–0.69). The present results shows that (r_A/r_O= 0.483–0.505) and (r_B/r_O= 0.494–0.497) satisfying the argument.

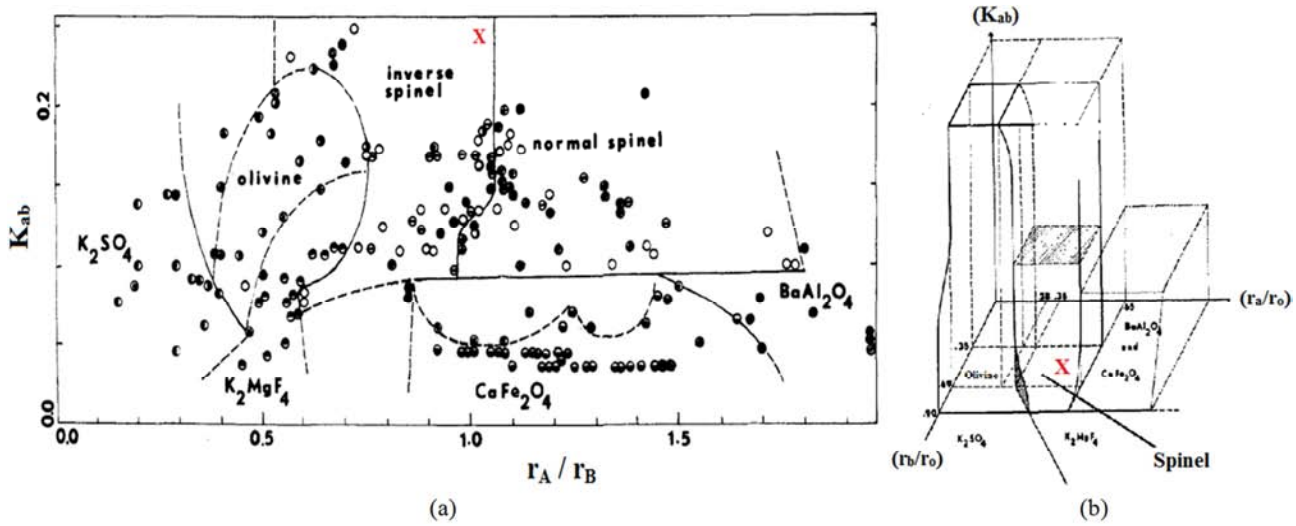

Figure 22. *(a): The K_{AB} versus r_A/r_B for spinel system (ref. 39). X represents the position of the present $Mg_{1-x}Zn_xFeNiO_4$ spinels. (b): shows three dimensional diagram of K_{AB} versus r_A/r_O and r_B/r_O. X represents the position of the present $Mg_{1-x}Zn_xFeNiO_4$ spinels.*

The samples surface morphology has been characterized using analytical scanning electron microscope (ASEM) model JSM-6510LA-JEOL and transmission electron microscope model JEM-1400-JEOL. The samples were prepared by drop coating from alcohol dispersion on the copper grids using ultrasound. The SEM and TEM micrographs of the $Mg_{1-x}Zn_xFeNiO_4$ spinels are shown in Figure 23 and Figure 24 respectively. It appears that the sample surfaces composed of approximately spherical to cubic grains. It also shows a well-packed and continuous grain structure with porosity and small holes at the grains boundaries. There is agglomeration phenomenon in the grains, which forms large grains. The SEM micrographs clearly showed aggregates of well-defined stacked grains of up to few mm in size, which might be caused by the high temperatures (>1000°C) heat treatment for long time (24h). Grain sizes obtained from SEM and TEM micrographs are larger than those obtained from the XRD calculations using Debye-Scherer's equation and Williamson-Hall plot [45]. Similar results have been shown by other spinels such as $Mg_{1-x}Zn_xFe_2O_4$ [21] spinels such as $ZnFe_{2-x}Cr_xO_4$ [22], $MgCr_xFe_{2-x}O_4$ [24], $Zn_{1-x}Cd_xFe_2O_4$ [48] and $Mg_{1-x}Zn_xFeCrO_4$ [34].

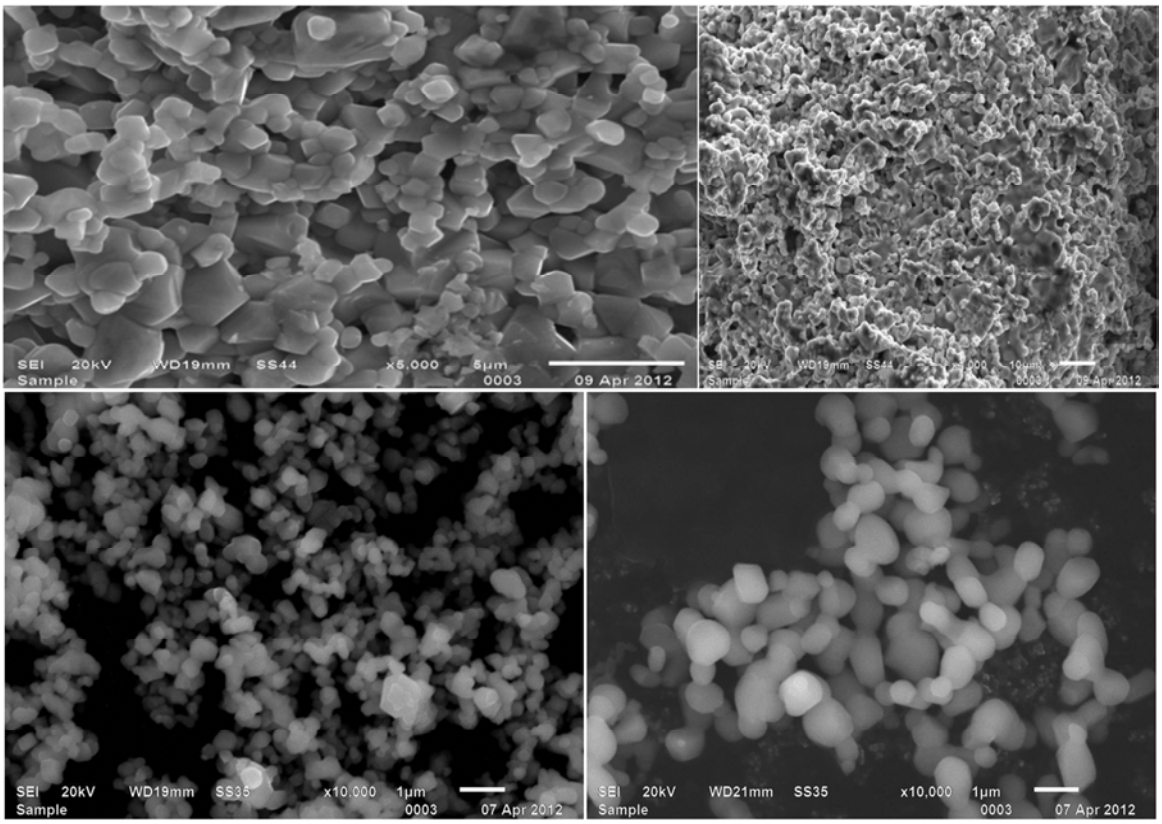

Figure 23. *The SEM images for the $Mg_{1-x}Zn_xFeNiO_4$ spinels.*

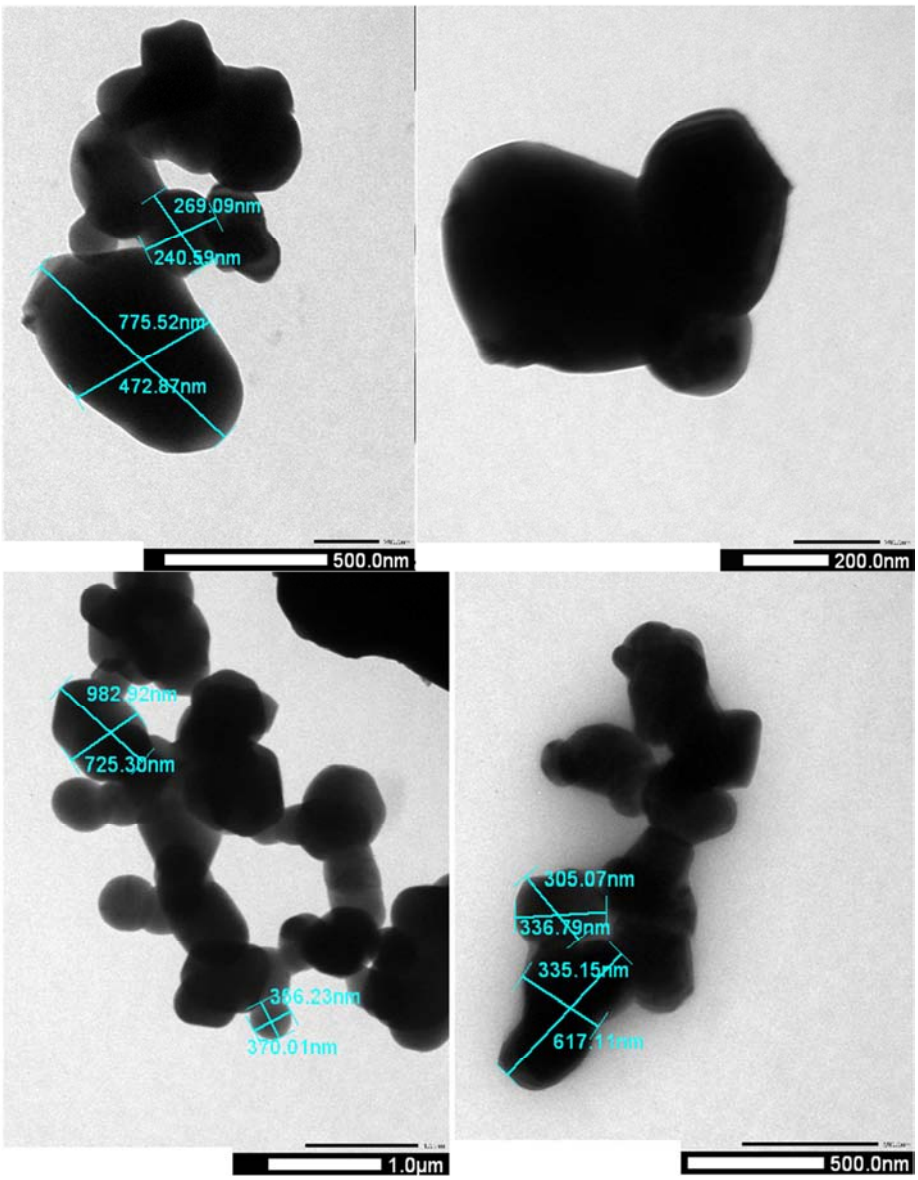

Figure 24. *The TEM images for the for the $Mg_{1-x}Zn_xFeNiO_4$ spinels.*

4. Conclusions

The $Mg_{1-x}Zn_xFeNiO_4$ spinels have been prepared using the solid state sintering techniques with sintering temperatures about 1100°C. Both the XRD and FTIR analyses confirm the formation of the face centered cubic spinel phase. The replacement of Mg ions with Zn ions influences the properties of these spinels. Most of the structural parameters such as the lattice constant, bond lengths, the infrared band centers, the oxygen positional parameter and the inversion factor increase as Zn content increases. Values of the ordering, inverse and randomness parameters moves towards the spinel structure normality as the Zn content (x) increases in the sample. The sample $MgFeNiO_4$ has the complete randomness configuration with an order parameter of about (2/3) and its composition can be written as $(Mg_{1/3}Fe_{2/3})_A[Mg_{2/3}Fe_{1/3}Ni_{3/3}]_BO_4$. This satisfies the fact that the more inverse the spinel the more the disorder. The lattice constant increases with increase in Zn content. This has been attributed to the replacement of smaller Mg^{2+} (0.66Å) cations with a larger cation, the Zn^{2+} of ionic radius (0.74Å). The estimated crystallite sizes were found to depend on the type of estimation method and on the Zn constant (x). Values of the crystallite sizes were found to be in the ranges (26-34) nm, (61-102) nm and (of order of few mm) for the D-S, W-H and SEM methods respectively. Values of the relative integrated areas under the peak vary in the same manner, the areas increase as Zn content increases. Unlike the areas the ratios of the calculated to the observed diffracted X-ray intensities vary in different manner with Zn contents. The Debye-Waller factors were estimated to be in the range (0.77-1.44 A^2) with a free strain DWF value of (0.513A^2) in these spinels. Values of Debye temperature decrease as the Zn^{2+} content increase in the sample. This might be caused by the enhancements of the lattice vibrations, which causes reduction of the Debye temperatures. Another reason might

be the increase of the average masses, which have an inverse relation with θ_D values. Most of the investigated properties such as the oxygen positional factor, Debye Waller factor, crystallite sizes and many others parameters were found to fall into two separate regions; the first region (largely normal) at (0.0 – 0.6) and the second region (largely inverse) at (0.6 – 1.0). These behaviours reflect the differences in nature of the structural phases between the two regions in these samples.

Declaration

1) The article is original.
2) The article has been written by the stated authors who are ALL aware of its contents and approve its submission.
3) The article has not been published previously.
4) The article is not under consideration for publication elsewhere
5) No conflict of interest exists, or if such conflict exists, the exact nature must be declared.
6) If accepted, the article will not be published elsewhere in the same form, in any language, without the written consent of the publisher.

References

[1] Alex Golden (2006) "Applications and Functions of Ferrites". In: Modern Ferrite Technology. Springer, Boston, MA. USA

[2] K. K. Kefeni, T. A. M. Msagati and B. B. Mamba "Ferrite nanoparticles: Synthesis, characterization and applications in electronic device" materials Science and Engineering Vol. 215 (2017) 37-55. https://doi.org/10.1016/j.mseb. 2016.11.002

[3] J. M. Hastings and L. M. Corliss "Neutron Diffraction Studies of Zinc Ferrite and Nickel Ferrite" Rev. Mod. Phys. Vol. 25 (1953) 114-118 https://doi.org/ 10.1103/RevModPhys.25.114

[4] P. K. Nayak "Synthesis and characterization of cadmium ferrite" Mater. Chem. Phys. Vol. 112 (2008) 24–26 http://doi:10.1016/j.matchemphys 2008.05.018

[5] C. P. Marshall, W. A. Dollase "Cation arrangement in iron-zinc-chromium spinel oxides"Ameri. Miner. Vol. 69 (1984) 928-936.

[6] L. M. Corliss, J. M. Hastings, and F. G. Brockman "A Neutron Diffraction Study of Magnesium Ferrite" Phys. Rev. Vol. 90 (1953) 1013 –1018 https://doi.org/10.1103/ PhysRev.90.1013

[7] H. Knoch, H. Dannheim "Temperature dependence of the cation distribution in magnesium ferrite" Phys. Status. Solidi A 37 (1976) K135-K137.

[8] https://doi.org/10.1002/pssa.2210370251

[9] D. Carta, M. F. Casula, A. Falqui, D. Loche, G. Mountjoy, C. Sangregorio and A. Corrias "A structural and magnetic investigation of the inversion degree in ferrite nanocrystals MFe_2O_4 (M) Mn, Co, Ni)" J. Phys. Chem. C 113 ((2009) 8606–8615. https://doi:10.1021/jp901077c

[10] C. Angelettfir, F. Pepe and P. Porta "Structure and catalytic activity of $CoMg_{1-x}A1_2O_4$ spinel solid solutions. Part 1: cation distribution of Co^{2+} ions" J. Chem. Soc., Faraday Trans. 1, Vol. 73 (1977) 1972-1982. https://www.doi0.1039/F19777301972

[11] P. Porta, A. Anichini, U. Bucciarelli "Distribution of nickel ions among octahedral and tetrahedral sites in $Ni_xZn_{1-x}Al_2O_4$ spinel solid solutions". J. Chem. Soc. Faraday Trans. Vol. 1 (1979) 1876-1887. https://doi.10.1039/ F19797501876

[12] Hugh St. C. O'Neill and Alexandra Navarotsky "Simple spinels: crystallographic parameters, cation radii, lattice energies, and cation distribution" Amer. Miner. Vol. 68 (1983) 181-194

[13] A. M. Gismelseed, K. A. Mohammed, F. N. Al-Mabsali, M. S. Al-Maashani, A. D. Al-Rawas, A. A. Yousif, H. M. Widatallah, M. E. Elzain. "The effect of Zn substitution on the structure and magnetic properties of magnesium nickel ferrite" Hyperfine Interact Vol. 239: 16 (2018). https://doi.org/10.1007/s10751-018-1492-4

[14] Y. Waseda, E. Matsubara, K. Shinoda, X-ray Diffraction Crystallography, Springer-Verlag Berlin, Heidelberg, 2011

[15] A. R. Jani and V. B. Gohel "Temperature variation of Debye-Waller factor for alkali and nobel metals" Z. Naturforsch Vol. 38 a (1983) 503-508

[16] N. Singh and P. K. Sharma "Debye-Waller Factors of Cubic Metals" Phys. Rev. B 3 Vol. 1141 (1971). https://doi.org/10.1103/ PhysRevB.3.1141

[17] H. L. Kharoo, O. P. Gupta, M. P. Hemkar, "Debye Waller factors in bcc metals. I" J. Phys. Soc. Jap. Vol. 43 (1977) 797-799. https://doi.org/10.1143 /JPSJ.43.2030

[18] H. L. Kharoo, O. P. Gupta, M. P. Hemkar, Debye Waller factors of fcc metals by the modified angular force model, Z. Naturforsch. 32 a (1977) 570-576. ISSN 0932-0784

[19] O. P. Gupta "Debye-Waller Factors of Nickel, Aluminium and Sodium" J. Phys. Soc. Jpn. 38 (1975) 1451-1454 https://doi.org/10.1143/JPSJ.38.1451

[20] J. Prakash, L. P. Pathak and M. P. Hemkar "Debye-Waller factor of α-Iron and Sodium" Aust. J. Phys. Vol. 28 (1975) 63-68

[21] J. Bashir, N. M. Buit, M. NasirKhan and Q. H. Khan "Determination of the Debye-Waller Factor of Molybdenum by Powder Neutron Diffraction" J. Appl. Cryst.Vol. 25 (1992) 797-799. https://doi.org/10.1107/S0021889892007416

[22] K. A. Mohammed, A. D. Al Rawas, A. M. Gismelseed, A. Sellai, H. M. Widatallah, A. Yousif, M. E. Elzain, M. Shongwe, Infrared and structural studies of $Mg_{1-x}Zn_xFe_2O_4$ ferrites, Physica B 407 (2012) 795-804. 10.1016/j.physb.2011.12.097

[23] Kadhim A. M. Khalaf, A. D. Al Rawas, A. M. Gismelssed, Ahmed Al Jamel, Salwan K. J. Al Ani, M. S. Shongwe, K. O. Al Riyami and S. R. Al Alawi Influence of Cr substitution on Debye-Waller factor and relatedstructural parameters of $ZnFe_{2-x}Cr_xO_4$ spinels" J. Alloy Comp. Vol. 701 (2016) 474-486 https://doi.org/ 10.1016/ j.jallcom.2017.01.083

[24] B. D. Cullity "Elements of X-ray Diffraction" Addison-Wesley Publishing Company, Inc. 1959.

[25] K. Sabri, R. Rais, K. Taibi, M. Moreau, B. Ouddane, A. Addou, Structural Rietveld refinement and vibrational study of $MgCr_xFe_{2-x}O_4$ spinel ferrites, Phys. B 501 (2016) 38-44. https://doi.org/10.1016/j.physb. 2016.08.011

[26] A. Baykal, S. Eryigit, M. Sertkol, S. Unlu, A. Yildiz and S. E. Shirsath, " The effect of Cr^{3+} substitution on magnetic properties of $CoFe_2O_4$ nanoparticles synthesized by microwave combustion route" J. Supercond. Nov. Magn. Vol. 29 (2016) 2395-2400. https://doi.org/10.1007/s10948-016-3533-z

[27] P. P. Hankare, U. B. Sankpal, R. P. Patil, I. S. Mulla, R. Sasikala, A. K. Tripathi, K. M. Garadkar "Synthesis and characterization of nickel substituted cobalt ferrite nanoparticles by sol–gel auto-combustion method" J. Alloy. Comp. Vol. 553 (2013) 383–388. https://dx.doi.org/10.1016/j.jallcom.2012.11.181

[28] T. R. Tatarchuk, M. Bououdina, W. Macyk, O. Shyichuk, N. Paliychuk, I. Yaremiy, B. Al-NajarandM. Pacia "Structural, optical and magnetic properties of Zn-doped $CoFe_2O_4$ nanoparticles" Nano.Resea. Lett. Vol. 12 (141) (2017) 1-11. https://doi.org/10.1186/s11671-017-1899-x

[29] N. Murali, S. J. Margarette, G. P. Kumar, B. Sailaja, S. Y. Mulushoa, P. Himakar, B. K. Babu, V. Veeraiah "Effect of Al substitution on the structural and magnetic properties of Co-Zn ferrites" Physica B: Cond. Matt. Vol. 522 (2017) 1-6 https://doi.org/10.1016/j.physb.2017.07.043

[30] A. Globus, H. Pascard, V. Cagan "Distance between magnetic ions and fundamental properties in ferrites" J. Phys. Colloq. 38 C1 (1977) 163-168. https://hal.archives-ouvertes.fr/jpa-00216992

[31] R. D. Shannon "Revised Effective Ionic Radii and Systematic Studies of Interatomie Distances in Halides and Chaleogenides" Acta Cryst. A32 (1976), 751-767 https://doi.org/10.1107/S0567739476001551

[32] K. A. M. Khalaf, A. D. Al-Rawas, H. M. Widatallah, K. S. Al-Rashdi, A. Sellai, A. M. Gismelseed, Mohd. Hashim, S. K. Jameel, M. S. Al-Ruqeishi, K. O. Al-Riyami, M. Shongwe, A. H. Al-Rajhi "Influence of Zn^{2+} ions on the structural and electrical properties of $Mg_{1-x}Zn_xFeCrO_4$ spinels" J. Alloy. Comp. Vol. 657 (2016) 733-747. https://dx.doi.org/10.1016/j.jallcom.2015.10.157

[33] M. C. Chhantbar, U. N. Trivedi, P. V. Tanna, H. J. Shah, R. P. Vara, H. H. Joshi, K. B. Modi "Infrared spectral studies of Zn-substituted $CuFeCrO_4$ spinel ferrite system" Indian J. Phys. 78A (2004) 321-326. https://core.ac.uk/download/pdf/49286685.pdf

[34] H. M. Zaki, H. A. Dawoud "Far-infrared spectra for copper–zinc mixed ferrites" Physica B Vol. 405 (2010) 4476–4479. https://doi:10.1016/j.physb.2010.08.018

[35] S. Singhal, S. Bhukal, J. Singh, K. Chandra, S. Bansal "Optical, X-ray diffraction, and magnetic properties of the cobalt-substituted nickel chromium ferrites $CrCo_xNi_{1-x}FeO_4$ (x=0, 0.2, 0.4, 0.6, 0.8, 1.0) synthesized using sol-gel autocombustion method" J. Nano. Technol. 2011 (2011) 1-6. https://dx.doi.org/10.1155/2011/930243

[36] A. K. M. Zakaria, M. A. Asgar, S.-G. Eriksson, F. U. Ahmed, S. M. Yunus, A. K. Azad, H. Rundlof "Preparation of Zn substituted Ni-Fe-Cr ferrites and study of the crystal structure by neutron diffraction" Mater. Lett.Vol.(57) (2003) 4243-4250. https://doi.org/10.1016/S0167-577X(03)00298-2

[37] K. J. Standley, Oxide Magnetic Materials, Claredon Press, Oxford, 1990. ISBN 10: 0198513186 / ISBN 13: 9780198513186.

[38] R. J. Hill, J. R. Craig and G. V. Gibbs "Systematic of the spinel structure type" Phys. Chem. Miner. 4 (1979) 317-339. https://doi.10.1007/BF00307535

[39] B. F. Levine, "d-Electron effects on bond susceptibilities and ionicities" Phys. Rev. B Vol. 7 (1973) 2591-2599. https://doi.org/10.1103/PhysRevB.7.2591

[40] K. Kugimitu and H. Steikfink "The Influence of crystal radii and electronegativities on the crystallization of AB_2X_4 stoichiometries" Inorg. Chem. Vol. 7 (1968) 1762-1770. https://doi:10.1021/ic50067a015

[41] S. M. Patange, S. E. Shirsath, K. S. Lohar, S. G. Algude, S. R. Kamble, N. Kulkarni, D. R. Mane and K. M. Jadhav, "Infrared spectral and elastic moduli study of $NiFe_{2-x}Cr_xO_4$ nanocrystalline ferrites" J. Magn. Magn. Mater. Vol. 325 (2013) 107-111. https://doi.org/10.1016/j.jmmm.2012.08.022

[42] A. T. Raghavender, D. Pajic, K. Zadro, T. Milekovic, P. V. Rao, K. M. Jadhav and D. Ravinder "Synthesis and magnetic properties of $NiFe_{2-x}Al_xO_4$ nanoparticles" J. Magn. Magn. Mater. Vol. 316 (2007) 1-7. https://doi.org/10.1016/j.jmmm.2007.03.204

[43] Q. Lina, Y. Hea, J. Lina, F. Yang, L. Wang and J. Dong "Structural and magnetic studies of Mg substituted cobalt composite oxide catalyst $Co_{1-x}Mg_xFe_2O_4$" J. Magn. Magn. Mater. Vol. 469 (2019) 89–94. https://doi.org/10.1016/j.jmmm.2018.08.050

[44] S. Khanam, A. K. M. Zakaria, M. H. Ahsan, T. K. Datta, S. Aktar, S. I. Liba, S. Hossain, A. K. Das, I. Kamal, S. M. Yunus, D. K. Saha, S.-G. Eriksson "Study of the Crystallographic and Magnetic Structure in the Nickel Substituted Cobalt Ferrites by Neutron Diffraction" Mater. Sci. Appl. Vol. 6 (2015) Article ID: 55841, 10 pages. 10.4236/msa.2015.64038

[45] T. R. Tatarchuk, N. D. Paliychuk, M. Bououdina, B. Al-Najar, M. Pacia, W. Macyk and A. Shyichuk "Effect of cobalt substitution on structural, elastic, magnetic and optical properties of zinc ferrite nanoparticles" J. Alloys and Comp. Vol. 731 (2018) 1256-1266. https://doi.org/10.1016/j.jallcom.2017.10.103

[46] G. K. Williamsonand W. H. Hall "X-ray line broadening from filed aluminum and wolfram" Acta Metall, 1 (1953) 22-31. https://doi.org/10.1016/ 0001-6160(53)90006-6

[47] Gh. H. Khorrami, A. Khorsand Zak, A. Kompany and R. Yousefi "Optical and structural properties of X-doped (X=Mn, Mg, and Zn) PZT nanoparticles by Kramers–Kronig and size strain plot methods" Ceramic Inter. Vol. 38 (2012) 5683-5690. https://doi.org/10.1016/j.ceramint.2012.04.012

[48] A. Khorsand Zak and W. H. Abd. Majid "Characterization and X-ray peak broadening analysis in PZT nanoparticles prepared by modified sol-gel method" Ceramics Intern. Vol. 36 (2010) 1905-1910. https://doi.org/10.1016/j.ceramint. 2010.03.022

[49] M. Chakrabarti, D. Sanyal, A. Chakrabarti "Preparation of $Zn_{1-x}Cd_xFe_2O_4$ (x = 0.0, 0.1, 0.3, 0.5, 0.7 and 1.0) ferrite samples and their characterization by Mossbauer and positron annihilation techniques" J. Phys. Cond. Matter. 19 (2007) 236210 (11 pp). https://doi.org/10.1088/0953-8984/19/23/236210

[50] M. A. Tagliente and M. Massaro "Strain-driven (0 0 2) preferred orientation of ZnO nanoparticles in ion-implanted silica" Nuc.Instrum.methods in phys. Res. B 266 (2008) 1055–1061. https://doi:10.1016/j.nimb. 2008.02.036

[51] A. Khorsand Zak, W. H. Abd. Majid, M. E. Abrishami, RaminYousefi "X-ray analysis of ZnO nanoparticles by WilliamsoneHall and sizestrain plot methods" Solid State Sciences 13 (2011) 251-256. https://doi:10.1016/j.solidstatesciences. 2010.11.024

[52] M. Jalaly, M. H. Enayati, P. Kameli, F. Karimzadeh "Effect of composition on structural and magnetic properties of nanocrystalline ball milled $Ni_{1-x}Zn_xFe_2O_4$ ferrite" Physica B 405 (2010) 507–512 http://doi: 10.1016/j.physb.2009.09.044

[53] V. Sepelal, K. Tkacova, V. V. Boldyerv, S. Wissmann, K. D. Becke "Mechanically induced cation redistribution in $ZnFe_2O_4$ and its thermal stability" Physica B Vol. 234-236 (1997) 617-619. https://doi.org/10.1016/S09214526 (96)01061-7.

[54] M. H. Mahmoud, H. H. Hamdeh, A. I. Abdel-Mageed, A. M. Abdallah, M. K. Fayek "Effect of HEBM on the cation distribution of Mn-ferrite" Physica B Vol. 291 (2000) 49-53. https://doi.org/10.1016/S0921-4526(99)01381-2

[55] A. I. Borhan, T. Slatineanu, A. R. Iordan and M. N. Palamaru "Influence of chromium ion substitution on the structure and properties of zinc ferrite synthesized by sol-gel auto-combustion method" Polyhedron Vol. 56 (2013) 82-89 http://dx.doi.org/10.1016/j.poly.2013.03.058

[56] H. ST. C. O'Neill and A. Navrotsky "Simple spinels: crystallographic parameters, cation radii, lattice energies, and cation distribution" J. Am. Mineral., Vol. 68 (1983) 181–194.

[57] H. ST. C. O'Neill, M. James, W. A. Dollase and S. A. T. Redfern, "Temperature dependence of the cation distribution in $CuAl_2O_4$ spinel" Eur. J. Min. Vol. 17 (2005) 581-586.https://doi:10.1127/0935-1221/2005/0017-0581

[58] H. ST. C. O'Neill and W. A. Dollase "Crystal-structures and cation distributionsin simple spinels from powder XRD structural refinement -$MgCr_2O_4$, $ZnCr_2O_4$, Fe_3O_4 and the temperature-dependence of the cation distribution in $ZnAl_2O_4$" J. Phys. Chem. Miner. Vol. 20 (1994) 541-555. https://doi:10.1007%2FBF00211850

[59] S. M. Antao, I. S. Hassan, W. A. Crichton and J. B. Parise "Effects of high pressure and high temperature on cation ordering in magnesioferrite, $MgFe_2O_4$, using in situ synchrotron X-ray powder diffraction up to 1430 K and 6 GPa" Amer. Miner. Vol. 90 (2005) 1500 – 1505.

[60] A. Navrotsky and O. J. Kleppa "The thermodynamics of cation distributions in simple spinels" J. Inorg, Nucl. Chem. Vol. 29 (1967) 2701-2714 https://doi.org/10.1016/0022-1902(67)80008-3

[61] K. I. Lilova, C. I. Pearce, C. Gorski, K. M. Rosso and A. Navrotsky "Thermodynamics of the magnetite-ulvospinel (Fe_3O_4-Fe_2TiO_4) solid solution" Amer. Mineral. Vol. 97 (2012) 1330-1338. https://dx.doi:10.2138/am.2012.4076

[62] L. Schwarz, Z. Galazka, T. M. Gesing and D. Klimm, "On the influence of inversion on thermal properties of magnesium gallium spinel" Cryst. Res. Technol. Vol. 50 (2015) 961-966. https://doi:10.1002/cras.201500275

[63] V. Stevanovic, M. d'Avezac and A. Zunger "universal electrostatic origion of cation ordering in A_2BO_4 spinel oxide" J. Ameri. Chem. Soc. Vol. 133 (2011) 11649- 11654. https://dx.doi.org/10.1021/ja2034602

[64] (n.d.). Retrieved from http://shodhganga.inflibnet.ac.in/bitstream. 10603/ 151666/9/08_appendix.pdf

[65] H. Furuhashi, M. Inagaki, S. Naka "Determination of cation distribution in spinels by X- ray diffraction method" J. Inorh. Nucl. Chem. Vol. 35 (1973) 3009-3014. https://doi.org/10.1016/0022-1902(73)80531-7

[66] V. K. Lakhani, T. K. Pathak, N. H. Vasoya, K. B. Modi "Structural parameters and X-ray Debye temperature determination study on copper-ferrite-aluminate" Solid State Sci. Vol. 13 (2011) 539-547. https://doi.org/10.1016/j.solidstatesciences.2010.12.023

[67] E. F. Westrum Jr., D. M. Grimes "Low temperature heat capacity and thermodynamic properties of zinc ferrite" J. Phys. Chem. Solids Vol. 3 (1957) 44-49. https://doi.org/10.1016/0022-3697(57)90046-X

[68] G. C. Bensin and E. K. Gile, Tables of integral functions related to Debye-Waller factors (National Research Council of Canada, Ottawa) 1966.

[69] K. A. M. Khalaf, A. D. Al-Rawas, H. M. Widatallah, K. S. Al-Rashdi, A. Sellai, A. M. Gismelseed, Mohd. Hashim, S. K. Jameel, M. S. Al-Ruqeishi, K. O. Al-Riyami, M. Shongwe, A. H. Al-Rajhi "Influence of Zn^{2+} ions on the structural and electrical properties of $Mg_{1-x}Zn_xFeCrO_4$ spinels" J. Alloy Comp. 657 (2016) 733-747 https://doi.org/10.1016/j.jallcom.2015.10.157

[70] O. V. Lounassmaa and L. J. Sundstrom "Specific heat of Gadolinium, Terbium, Dysprosium, Holmium, and Thulium metalsbetween 3 and 25 K" Phys. Rev. Vol. 150 (1966) 399-412. https://doi.org/10.1103/PhysRev.150.399

[71] K. B. Modi, T. K. Pathak, N. H. Vasoya, V. K. Lakhani, G. J. Baldha, P. K. J ha "X-ray Debye temperature of mechanically milled $Ni_{0.5}Zn_{0.5}Fe_2O_4$ spinel ferrite" Indian J. Phys. Vol. 85 (2011) 411-420. https://doi.org/10.1007/s12648-011-0051-5

[72] B. Bridge and A. A. Higazy "Acoustic and optical Debye temperatures of thevitreous system CoO-Co_20_3-P_2O_5" J. Mater. Sci. Vol. 21 (1986) 2385-2390.

[73] https://doi.org/10.1007%2FBF01114282

[74] D. C. Gupta and M. N. Sharma "Infrared eigen frequency and characteristic Debye temperature of a few heavier halides" Indian journal of Physics Vol. 43 (1969) 201-204

[75] R. D. Waldron, Infrared spectra of ferrites, Phys. Rev. 99 (1955) 1727-1735. https://doi.org/10.1103/PhysRev.99.1727

[76] C. M. Srivastava and T. T. Srinivasan 'Effect of Jahn-Teller distortion on the lattice vibration frequencies of nickel ferrite" J. Appl. Phys. 53 (1982) 8148-8150. http://dx.doi.org/10.1063/1.330276

[77] S. A. Patil, V. C. Mahajan, A. K. Ghatage and S. D. Lotke "Structure and magnetic properties of Cd and Ti/Si substituted cobalt ferrites" Mater. Chem. Phys. Vol. 57 (1998) 86-91. https://doi.org/10.1016/S0254-0584(98)00202-8

[78] T. Satoh, T. Tsushima, K. Kudo, A classification of normal spinel type compounds by "Ionic packing factor" Mater. Res. Bull. 9 (1974) 1297-1300. https://doi.org/10.1016/0025-5408(74)90051-8

[79] R. L. Williams "The relation of force constant to electronegativity and covalent radius" J. Phys. Chem. Vol. 60 (1956) 1016–1017. https://doi:10.1021/j150541a050

[80] W. Gordy "A Relation between Bond Force Constants, Bond Orders, Bond Lengths, and the Electronegativities of the Bonded Atoms" J. Chem. Phys. Vol. 14 (1946) 305-320. https://doi.org/10.1063/1.1724138